PRODUCTION AND CHARACTERIZATION OF Ti-BASED MXENE ALLOYS

MERVE ÖZKAN

MAY 2023

ÇANKAYA UNIVERSITY

GRADUATE SCHOOL OF NATURAL AND APPLIED SCIENCES

DEPARTMENT OF MATERIALS SCIENCE AND ENGINEERING
M.Sc. Thesis in
MICRO AND NANO TECHNOLOGY

PRODUCTION AND CHARACTERIZATION OF Ti-BASED MXENE ALLOYS

MERVE ÖZKAN

MAY 2023

ABSTRACT

PRODUCTION AND CHARACTERIZATION OF Ti-BASED MXENE ALLOYS

ÖZKAN, MERVE
M.Sc. in Micro and Nanotechnology

Supervisor: Assoc. Prof. Dr. Ziya ESEN
Co-Supervisor: Prof. Dr. Arcan F. DERİCİOĞLU
May 2023, 72 Pages

In this study, production and characterization studies were carried out for both Ti_3AlC_2 MAX and $Ti_3C_2T_x$ MXene alloy powders, and their foam counterparts. Firstly, MAX alloy powders were obtained by grinding and sieving via utilizing the Ti_3AlC_2 MAX alloy produced by powder metallurgy. Afterwards, $Ti_3C_2T_x$ MXene alloy powders were synthesized by chemical etching method using both commercial and lab produced MAX alloy powders. In order to investigate the apatite formation ability using simulated body fluid, MAX alloy foams with around 45% porosity were produced using space holder method. On the other hand, MXene alloy foams were obtained by etching of produced MAX alloy foams. Synthesized MXene powders were added to polyvinyl alcohol by 1, 5 and 10 wt.% and their antibacterial properties were determined.

Ti_3AlC_2 MAX powders, produced by grinding and sieving of sintered MAX alloy compacts at 1400 ^oC, displayed mainly Ti_3AlC_2 phase and in contrast to commercial MAX alloy powders, very small amount of TiC phase formed in lab produced alloy powders. In both types of MAX alloy powders, etching with HF acid decreased the average powder particle size. Although layered structure was formed as a result of selective etching of Al in commercial MAX alloy powders, similar structure didn’t form in lab produced powders. Ultrasonication, applied to obtained thinner MXene layers, resulted in oxidation of the powders. MXene alloy powder added polyvinyl alcohol composites displayed higher antibacterial resistance to Escherichia coli gram negative bacteria with increased MXene powder content. On the other hand, MXene alloy foams didn’t allow apatite formation even after 25 days. However, MAX alloy foam allowed apatite formation after 15 days; therefore, it is concluded that MAX alloy foams can be considered as candidate materials in bone graft applications.

Keywords: Ti_3AlC_2 MAX alloy, $Ti_3C_2T_x$ MXene alloy, Foams, Apatite formation, Antibacterial test.

ÖZET

TİTANYUM ESASLI MXENE ALAŞIMLARININ ÜRETİMİ VE KARAKTERİZASYONU

ÖZKAN, MERVE
Mikro ve Nanoteknoloji Yüksek Lisans

Danışman: Prof. Dr. Ziya ESEN
Ortak Danışman: Prof. Dr. Arcan F DERİCİOĞLU
Mayıs 2023, 72 Sayfa

Bu çalışmada Ti_3AlC_2 MAX ve $Ti_3C_2T_x$ MXene alaşım tozlarının sentezlenmesi ile birlikte biyomedikal uygulamalar için gözenekli yapıda Ti_3AlC_2 MAX ve $Ti_3C_2T_x$ MXene alaşımlarının üretimi ve karakterizasyonu gerçekleştirilmiştir. İlk olarak toz metalurjisi ile üretilen Ti_3AlC_2 MAX alaşımlarından öğütme ve eleme yöntemi ile toz elde edilmiş, ardından hem ticari, hem de çalışmada üretilen MAX tozları kullanılarak kimyasal dağlama yöntemi ile $Ti_3C_2T_x$ MXene alaşım tozları sentezlenmiştir. Yapay vücut sıvısı kullanılarak apatit oluşumunu araştırmak için yaklaşık % 45 gözeneğe sahip MAX alaşım köpükleri boşluk yapıcı metodla MAX alaşım tozları kullanılarak üretilmiştir. MXene alaşım köpükleri ise üretilen MAX alaşım köpüklerinin kimyasal dağlanması ile elde edilmiştir. MAX tozundan üretilmiş olan MXene tozları ise ağırlıkça % 1, 5 ve 10 oranlarında polivinil alkol ile karıştırılarak tozun antibakteriyel özellikleri belirlenmiştir.

1400 ^{o}C sıcaklıkta sinterleme sonucu öğütme ile üretilen Ti_3AlC_2 MAX tozlarında Ti_3AlC_2 fazı ile ticari tozların aksine çok az miktarda TiC fazına rastlanmıştır. HF asit ile dağlanma işlemi ticari ve laboratuvar üretimi MAX tozlarının ortalama tane büyüklüğünü düşürmüştür. Al elementinin dağlanması sonucu ticari MAX tozlarından katmanlı MXene tozları sentezlenmiş, fakat laboratuvar üretimi MAX tozlarında bu yapılara rastlanmamıştır. İnce MXene katmanları oluşturmak için uygulanan ultrasonik işlem ise tozların oksitlenmesine neden olmuştur. MXene katkılanarak üretilmiş polivinil alkol esaslı kompozitlerle yapılan testlerde MXene miktarının artışıyla kompozitin Escherichia coli gram negatif bakterisine karşı antibakteriyel özelliğinin arttığı gözlemlenmiştir. Diğer taraftan MXene alaşım köpüklerinin 25 gün sonunda dahi apatit oluşumuna olanak sağlamadığı tespit edilmiştir. MAX alaşım köpüklerinin ise 15 gün sonunda apatit oluşumuna olanak sağladığı ve kemik grefti uygulamalarında aday malzeme olarak değerlendirilebileceği görülmüştür.

Anahtar Kelimeler: Ti_3AlC_2 MAX alaşımları, $Ti_3C_2T_x$ MXene alaşımları, Köpükler, Apatit oluşumu, Antibakteriyel test.

To My Precious Dad,

ACKNOWLEDGEMENT

I would like to express my sincere gratitude to my remarkable supervisor Prof.Dr. Ziya Esen, who encouraged me to start my graduate education and guided my academic life with his unique experience. I would like to thank him for his extraordinary patience, endless motivation, and invaluable support throughout all the time of my research. I could not have imagined writing this thesis without his motivation and mentorship.

I would like to express my gratitude and thanks to my co-supervisor Prof. Dr. Arcan F. Dericioğlu for his help and wisdom during my graduate studies.

I want to express my profound thanks to Assist. Prof. Şeniz Seyhan Kuşhan Akın. Throughout this period, she helped me in many ways and shared her knowledge and opinions about my studies.

I am eternally grateful to dear Ezgi Bütev Öcal for sharing her vast experiences with me, guiding me, and always supporting me.

I would also like to thank Assist. Prof. Dr. Kemal Davut for his many helps in this study.

I would like to thank my friends Seren Özer and Merve Nur Doğu for sharing their experiences with me and for their endless help.

I would like to express my deepest gratitude to my lovely friendships Sıla Büyükatak and Rabia Ediz, who helped me both physically and morally during this process.

I would like to thank my dear friends Berna, Ebru, Kübra, Dicle, Işılay and Mert Battal, who have always supported me throughout this process.

I am also grateful to my laboratory mates and friends, Ertuğrul Büyükhergül and Aybüke Öztürk for their help and wise suggestions.

I would like to specially thank all technical staff at Middle East Technical University, Atılım University and Çankaya University for their helps

Special thanks to my dear mother Sevim Özkan for her endless patience, efforts, and love. I would like to thank my dear sisters Figen and Gönül for always being there for me and their support.

Finally, I would like to express my deepest gratitude to my precious father Zekai Özkan, who has always given me his love, support, patience and made me who I am throughout his life.

In addition, I would like to thank you for being financially supported by the Tübitak SAYEM 3219504 project.

TABLE OF CONTENTS

LIST OF TABLES

LIST OF FIGURES

CHAPTER I

INTRODUCTION

Two-dimensional (2D) materials have emerged as attractive alternatives to graphene in several fields of application since the discovery of monolayer graphene synthesized from three-dimensional (3D) graphite in 2000. The discovery of new 2D materials has become a necessity due to the possibility of improving the quality of life by use of 2D materials in many technological fields. MXene alloys, which have been included in the world of two-dimensional materials since 2011, have recently attracted a lot of attention by researchers since they provide diverse properties.

The 2D MXene alloys, consisting of elements like transition metals, carbon, and nitrogen, have started a new era in nanotechnology. In addition to having a layered structure, with adjustable surface terminations, they exhibit many excellent electrical, thermal, and optical properties. Thanks to these features, their applicability in many areas like biomedical, energy and sensor technology are still being investigated the implementation of MXene alloys as composites has also made it possible to assemble conventional devices and achieve more effective outcomes in biomedical, energy, and sensor applications due to their high surface areas and customizable surface terminations.

MXene alloys are synthesized from MAX alloys with a three-dimensional structure using various etchants, usually by selective wet etching method. $M_{n+1}X_nT_x$ MXene alloy is obtained by eliminating the layer consisting of ‘A’ element in the $M_{n+1}AX_n$ type MAX alloys. The etching solutions and the type of methods used for synthesizing MXene alloys lead to different properties in the produced due to differences in size, shape, number of layers and surface terminations obtained. Additionally, the starting type and properties of MAX alloys have a significant impact on the characteristics of final MXene alloys. The $Ti_3C_2T_x$ alloy, which was first found in 2011 and synthesized from the Ti_3AlC_2 MAX alloy, is the most popular MXene alloy studied so far. In addition, there are roughly 100 stoichiometric types of MXene alloys overall. In order to produce multilayer, few-layer, or single-layer $Ti_3C_2T_x$

MXene alloy with high efficiency and contamination-free, a variety of etchants, such as hydrofluoric acid (HF), hydrochloric acid (HCl), and various molten salt solutions have been utilized for breaking the weak Van der Waals bonds between titanium and aluminum. The efficiency of etching and obtaining single layer MXene still need to be improved. During synthesizing, MAX alloy powders are typically centrifuged with deionized water at a particular high speed for a particular period of time to remove the residues after etching for about 24 hours. The multilayer MXene alloys produced after centrifugation are then subjected to exfoliation processes, if desired, to reduce the number of layers., An intercalation process is used to obtain few layers of MXene by allowing penetration of ions of organic or inorganic molecules as dimethyl sulfoxide (DMSO) or urea between the layers, which expands and results in separation of layers. Following the intercalation process, sonication is found to be helpful in getting few or single layered MXene sheets.

The elements in MAX alloys, which are often used in elemental form during production via powder metallurgy techniques, can also affect the production procedure. Ti_3AlC_2 MAX alloy powder is mostly produced using the hot isostatic press, spark plasma sintering, high temperature sintering, and mechanical alloying techniques. However, the studies have demonstrated that the Ti_3AlC_2 MAX alloys, which were sintered at high temperature after mechanical alloying, provided the maximum efficiency in terms of obtaining single phase and the least amount of contamination. However, the production techniques of MAX alloys and MXene synthesizing by etching techniques still need to be improved.

Additionally, the studies have shown that $Ti_3C_2T_x$ MXene alloy has the ability to kill bacteria owing to its structure and surface termination group. The search for materials with antibacterial properties has become increasingly important, especially for the bacteria that have resistance to antibiotics. 2D materials like $Ti_3C_2T_x$ MXene alloy kills bacteria due to its structural properties. Additionally, the possibility of usage MXene and MAX alloys as a graft material to improve bone tissue ingrowth is questionable and needs to be investigated.

In this thesis, the literature about production, characterization, and applications of MAX and MXene alloys is given in Chapter 2. After that, the details of raw materials and methods used for manufacturing Ti_3AlC_2 MAX alloy, $Ti_3C_2T_x$ MXene alloy powder and their foam counterparts are given with the characterization and functional testing in Chapter 3. Chapter 4 describes the results and discussions of the subsequent investigations. Finally, important findings and future studies are presented in Chapter 5.

CHAPTER II

THEORETICAL BACKGROUND

2.1 NANOTECHNOLOGY

The design and controlled production of devices with at least one dimension in the range of 1-100 nm has been named as nanotechnology by the National Science Institution in the United States [1,2].

As a material gets closer to nanoscale dimensions, it has been noticed that physical and chemical properties of materials change [2]. Therefore, it is possible to produce nanomaterials with different dimensions to be used in different fields such as electronics, energy, biomedical, informatics, energy, textile, and food industries. Precise control of the shape and size of the nanomaterials enables tuning of the properties materials and increasing the performance of device manufactured using nanotechnology.

The emergence of quantization effects because of the confinement of electron movement is one of the most obvious consequences of reducing materials to the nanometer range [2].

2.1.1 Classification of Nanomaterials

In 2007, Pokropivyn and Skorokhod [3] developed a dimensional classification by considering the dimensions of the nanostructures and the structures they form. Accordingly, they classified the nanostructures as zero-dimensional (0D) one dimensional (1D), two-dimensional (2D) and 3-dimensional (3D) nanostructures [13]. Schematic dimensional demonstration of nanomaterials is given in Figure 1.

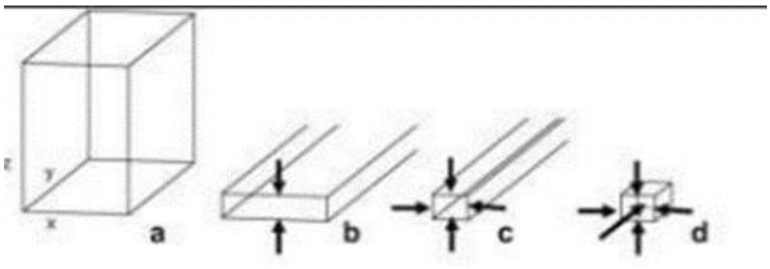

Figure 1: a) 3-dimensional structure, b) 2- dimensional thin film (layer structure, quantum well), c) 1- dimensional structure, d) 0- dimensional structure [4]

2.1.1.1 Zero – Dimensional Nanomaterials

Atomic clusters, filaments, and clusters such as quantum dots, nanoparticle array and core-shell nanoparticles (Figure 2) are examples of zero-dimensional (0D) nanomaterials [2]. These materials are smaller than 100 nm in size and have a length of nearly equal to their width. 0D nanoparticles come in a variety of shapes and can be found alone or as part of a matrix in metallic, ceramic, or polymeric forms [1,2,4].

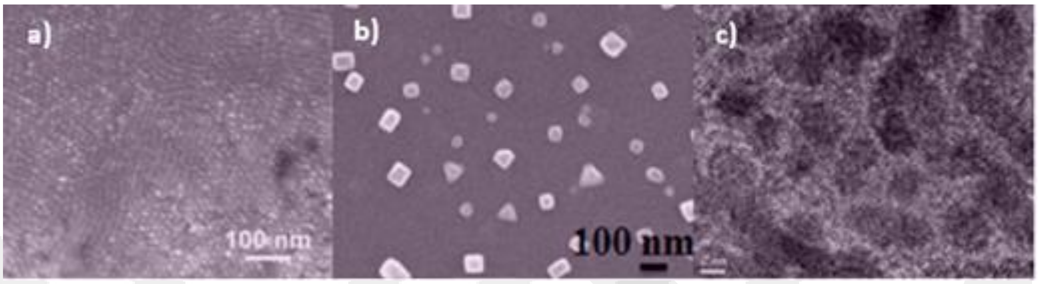

Figure 2: Scanning and Transmission electron microscopy images of 0D nanomaterials a) quantum dots, b) nanoparticles array, c) core-shell nanoparticles [1].

2.1.1.2 One – Dimensional Nanomaterials

The most common types of one-dimensional (1D) nanomaterials include nanorods, nanowires, nanotubes, and nanofibers (Figure 3). Both dimensions are measured in nanometers, with length being larger than their width [4]. Due to their two-dimensional confinement, electrons are unable to travel freely in two dimensions. Therefore, electronic, and optical properties change due to changes in energy band diagram of electrons. Therefore, 1D nanomaterials draw interest due to their structures in many fields including nano electronics, alternative energy sources, and nanodevices [2,4].

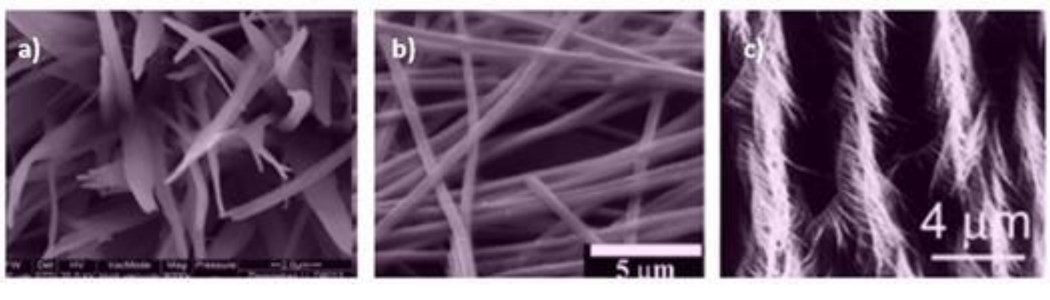

Figure 3: Scanning electron microscopy images of 1D nanomaterials, a) nanobelts, b) nanoribbons, c) hierarchical nanostructures [1].

2.1.1.3 Two- Dimensional Nanomaterials

Nanosheets, nanofilms, nanoprisms, and nanodisks are examples of twodimensional nanomaterials [2]. According to the synthesis process, it has a precise structure made up of one or more atomic layers, 2D nanomaterials, and its lateral dimensions can reach micrometer levels [5]. The features of 2D nanomaterials, such as electron trapping, optical qualities, anisotropy, appropriate surface area, and mechanical strength, seem promising. Due to their outstanding properties, they are used in energy, membrane, tissue engineering, medicine, and sensing applications [1, 2]. Figure 4 shows some of the popular 2D nanomaterials which has found great interest in recent years in the field of nanocomposite production, electronics, biomedical industry, etc. [5]. The invention of graphene in 2004—which was synthesized by extracting an atomically thin carbon layer from graphite—resulted sparking rise in 2D nanomaterials synthesis and applications. Since the graphene synthesis methods enable production of quantities in laboratory scale, the research on 2D materials displaying similar properties to that of graphene has risen in recent years.

For example, synthesis of MXene alloys from MAX alloys during 2010's by chemical methods are one of the examples on 2D nanomaterials production [5].

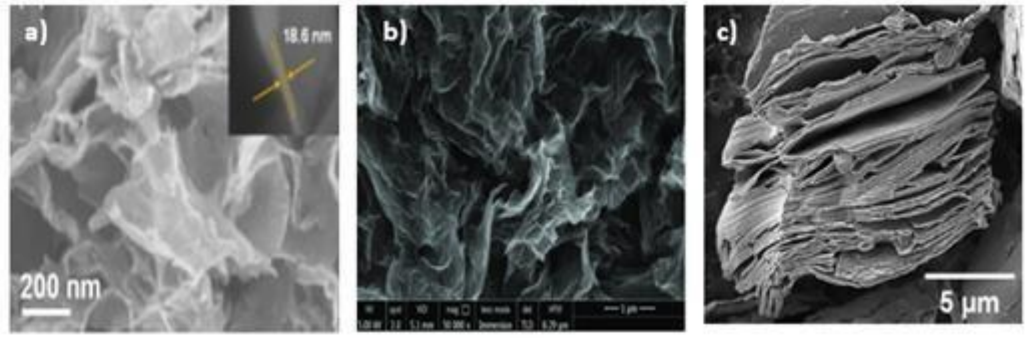

Figure 4: SEM images of various 2D nanomaterials, a) nanosheet, b) graphene, c) MXene [3].

2.1.1.4 Three- Dimensional Nanomaterials

3D nanomaterials (Figure 5), sometimes referred to as bulk nano materials, contain nano phase materials made up of coaxial grains with a diameter of a few nanometers [1]. The fundamental building blocks of 0D, 1D, or 2D nanocrystals are stacked to create 3D nanocrystals, which have bigger, more inventive designs. Additionally, electrons are unrestricted in all dimensions [2].

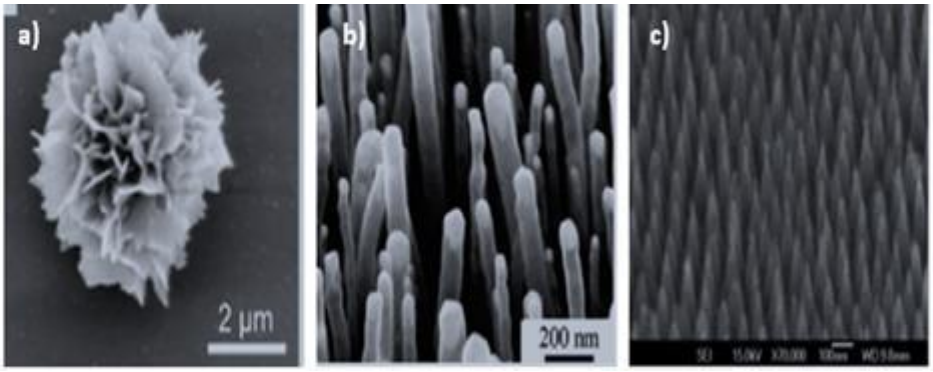

Figure 5: Typical three - dimensional nanomaterials, a) nanoflower [6], b) nanopillars [7], c) nanocones [1].

2.2 MAX ALLOYS

The MAX alloys are among the materials that have attracted attention for a long time with their properties and three-dimensional layered structures [8]. MAX phases show the binary behavior of both metals and ceramics. By this way, they show suitable thermal and electrical conductivity properties like metal, and they also have low density and high stiffness like ceramics [9]. Thanks to these high-performance features, it has the ability to offer a wide range of uses.

There are 60 types of MAX alloys known since the 1960s. The general chemical formula of MAX phase is as follows $M_{n+1}AX_n$, where n= 1, 2 or 3. As seen in the periodic table (Figure 6), M represents early transition metal elements, A represents group A elements, and X represents carbon or nitrogen, and it is a nanolayered ternary compound that has a hexagonal lattice structure, and their MAX phase space group is P63 /mmc [10]. The MAX phase's atomic arrangement likewise exhibits regularity. The MX lamellas and ‘A’ atom layer are stacked one on top of the other in the c direction to form the MAX phase (Figure 7). And two transition metal layers are placed between each X atom layer. Although the covalent bond between M and X is relatively strong in these structures, the bond between M and A is weak [10-13]. MAX alloys have the ability to have a distinctive layered structure at the nanoscale owing to their unique crystalline structure. The M_2AX, M_3AX_2, and M_4AX_3 phases are commonly referred to as 211, 312, and 413 phases, respectively, according to the value of “n” and in Figure 7 schematic representation of these structures is given [11]. Based on the differences between phases 211, 312 and 413, which are the most well-known phases of the MAX phases, there is a variation in the number of M layers between both

A layers [14-16]. In addition, the most known and studied compounds of these phases are given in Table 1, and Figure 8 shows SEM images of different MAX alloys.

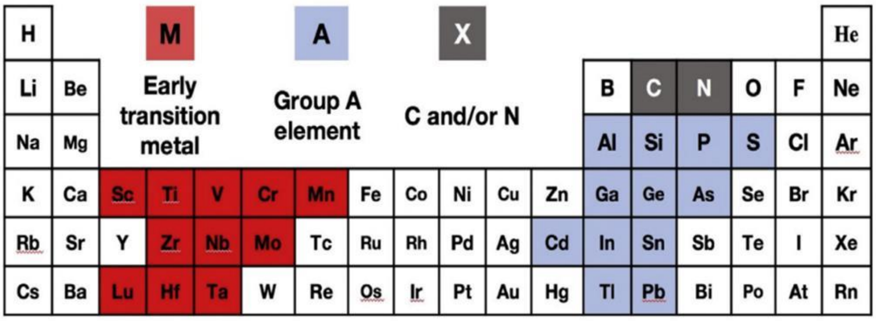

Figure 6: Elements used for MAX alloys in the periodic table [11].

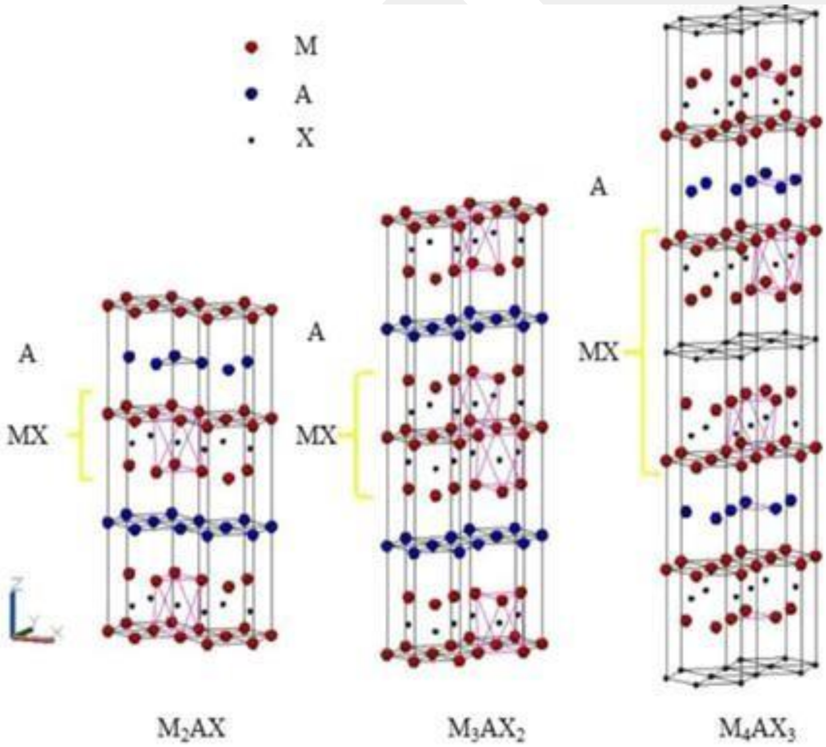

Figure 7: Representation of the structures of three different MAX phases with different "n" values [11].

Table 1: List of known 211, 312 and 413 MAX phases.

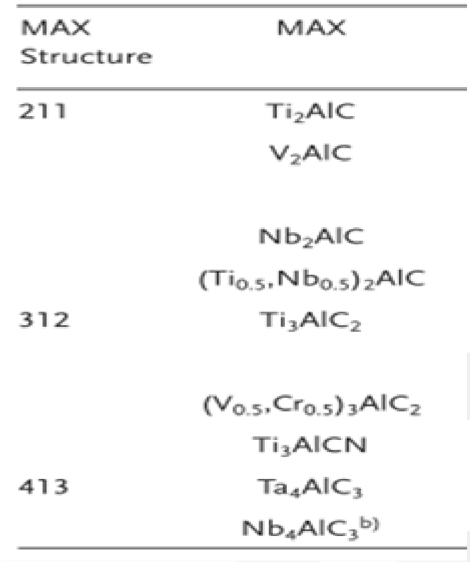

MAX Structure	MAX
211	Ti_2AlC
	V_2AlC
	Nb_2AlC
	$(Ti_{0.5},Nb_{0.5})_2AlC$
312	Ti_3AlC_2
	$(V_{0.5},Cr_{0.5})_3AlC_2$
	Ti_3AlCN
413	Ta_4AlC_3
	Nb_4AlC_3[b)]

The Ti_3AlC_2 is the most studied MAX alloy since the 1960s and has the classic '312' structure [16]. Ti_3AlC_2 has better plasticity at room temperature than other MAX alloys. It is resistant to damage and has received considerable attention since the 1960s for its incredible properties such as good machinability, low density (4.25 g/cm^3), low hardness, high elastic modulus, superior thermal shock resistance, high strength at high temperatures, low expansion coefficient, high oxidation resistance, self-lubricity attracts. Therefore, such properties make Ti_3AlC_2 a more attractive material and enables usage in many different areas [14]. Also, its high electrical conductivity, thermal conductivity and low frictional coefficient make it an extraordinary material.

Ti_3AlC_2 MAX alloys, which are generally produced using powder metallurgy methods, are produced using hot isostatic press (HIP), slip casting (SP), spark plasma sintering (SPS), self-propagating high-temperature synthesis (SHS) [13] and mechanical alloying methods. However, in the studies, it has been seen that it is difficult to produce in many production methods, generally with high purity, without contamination and without the presence of TiC, Al_2O_3 phases. On the other hand, it was observed that a purer Ti_3AlC_2 phase was obtained with the mechanical alloying method and the high temperature sintering method. At the same time, mechanical alloying and high-temperature sintering are advantageous to other methods in terms of being cheaper and obtaining a larger amount of Ti_3AlC_2 powder. [16].

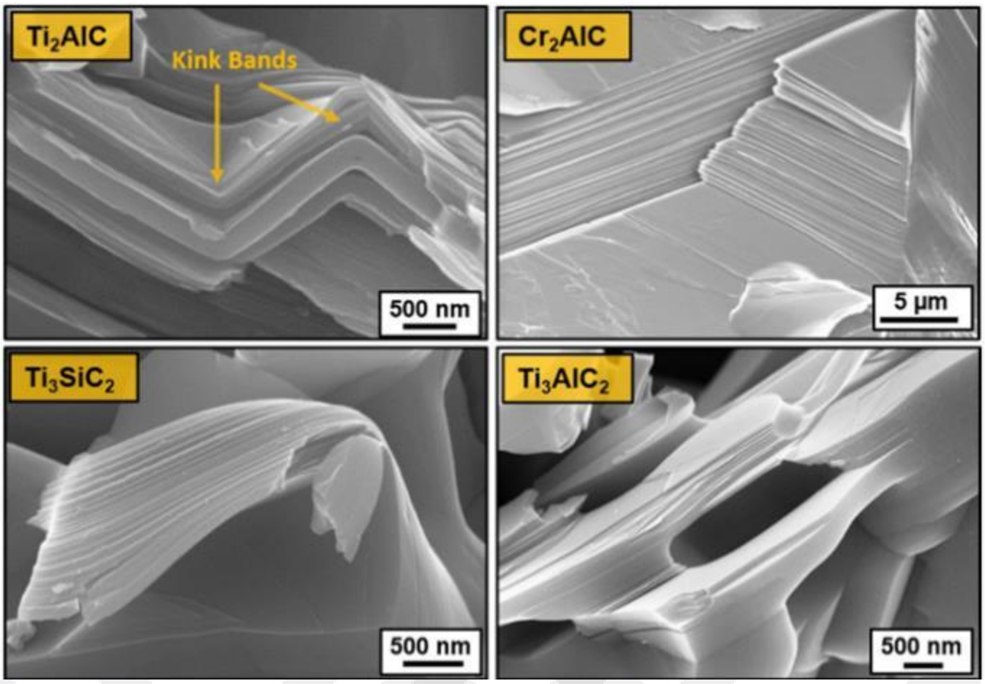

Figure 8: SEM pictures of Ti_2AlC, Cr_2AlC, Ti_3SiC_2 and Ti_3AlC2 MAX phases. Represented by [15].

2.3 MXENE ALLOYS

Two-dimensional (2D) materials have gained significant attention in the scientific community as a result of the discovery of graphene and its special qualities. A brand-new class of two-dimensional material known as MXene, which comprised transition metal carbides, nitrides, and carbonitrides, has recently come into existence. By removing specific layers of sp elements from three-dimensional (3D) phases known as MAX, these new 2D materials are created. The name of the MXene alloy, which was initially presented in 2011 at Drexel University, comes from its graphene-like structure and production from the MAX alloy. Since 2011, 100 different variants of the MXene alloy with 2D nano-layered structure obtained from the 3D structured MAX phases by exfoliation. Naguib et al. produced [17] MXene alloys for the first time in 2011 by exfoliating Ti_3AlC_2 MAX alloys. Since the bonds between the M-A atoms that make up the MAX alloy are weak, MXene alloys are synthesized by breaking of these bonds and by removing element A. The bonds are generally broken in acidic solutions and the obtained MXene alloy has the chemical formula of $M_{n+1}X_nT_x$ where M is an early transition metal (such as Sc, Ti, Zr, Hf, V, Nb, Ta, Cr, Mo, Mn), X is C and/or N, T is a surface termination unit (e.g., hydroxyl, oxygen or fluorine) formed during etching process and n = 1, 2, or 3 [10]. Figure 10 shows schematically $Ti_3C_2T_x$ MXene structure formation steps. Although MXene alloys are obtained from MAX alloys, they show completely different optical, electronic, electrochemical, and magnetic properties.

Accordingly, the research conducted on MXene alloys increases exponentially (Figure 9). It is a very promising 2D material to be used in various applications such as energy storage, sensors, catalysis, membranes, and biomedicine. Highly adjustable chemical and structural properties like unique electrical conductivity, thermal stability with its layered structure is just a few of superior features [10-17].

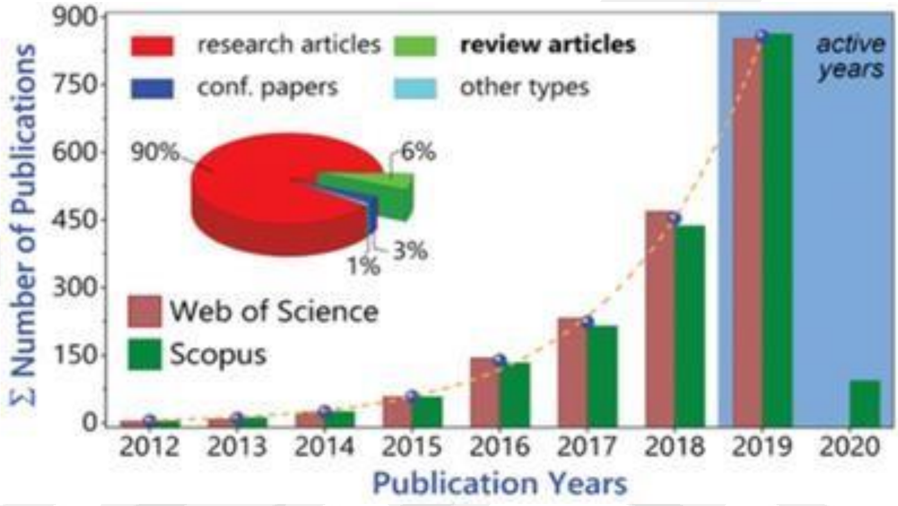

Figure 9: Graphical representation of MXene alloys studies [16].

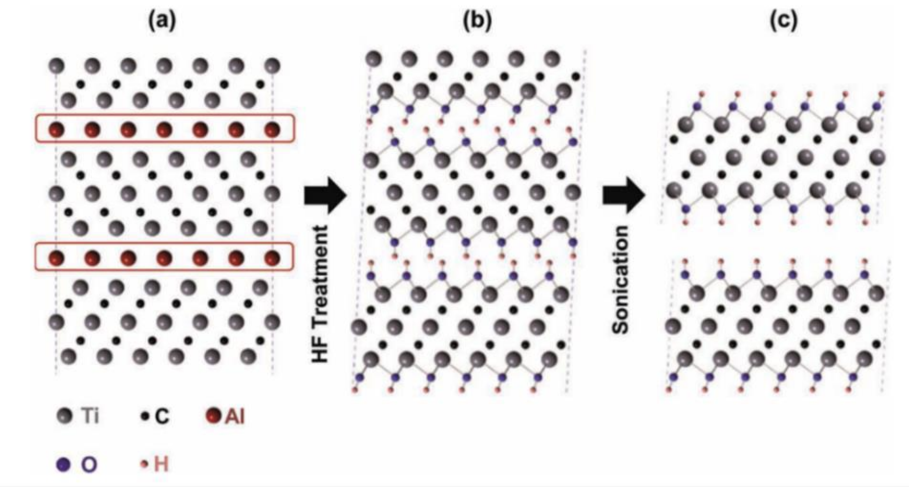

Figure 10: Schematical representation of $Ti_3C_2T_x$ MXene synthesis by HF etching of Ti_3AlC_2 MAX alloy [16].

MXene has highly variable and challenging physical and chemical properties which depends on stoichiometry and different surface functional groups obtained by use of different etchants [18]. For example, adjustable band gap, high electrical conductivity and capacity, large elastic modules, ultra-low optical attenuation, ability to intercalate ions, and compatibility with water and organic solvents have been demonstrated in studies to date. With these excellent features, MXene can be used efficiently in energy storage and conversion, catalysis, sensor, electronics, water purification and biomedical applications [16-18].

2.3.1 Synthesis of MXene

As noted above, MXenes are often derived from MAX alloys, where the M-A layers are weakly bonded together by a combination of covalent and metallic bonds [10-12]. It is known that there are 100 different MXene alloys synthesized so far, many of which have been obtained by eliminating the A layer. To break the M-A bonds of these different alloys, it is first necessary to find the right etchant that will eliminate the A layer.

In the MAX to MXene conversion, the eliminated layers are always replaced by various termination groups such as -OH, -O, -F, -Cl depending on the type of etchant [10-13].

Therefore, the material obtained after etching consists of $M_{n+1}X_nT_x$ multiple layers, which then can be separated to single graphene like nanosheets by intercalation methods in sonicated media [13].

The circumstances surrounding their synthesis have a significant impact on the composition and structure of MXene alloys. In a study [19], the structures of MXenes formed by varying the HF concentrations were examined, and it was discovered, as shown in Figure 11, that the gaps between the layers narrow as the HF concentration decreases. Additionally, it was discovered that the etch time can be affected by the acid concentration used. However, it was determined in a different study that the MXenes produced when the HF concentration was raised to 50 % possessed defects. As a result, several investigations have been published to produce MXene alloy with fewer defects by utilizing different etch solutions in place of HF [19].

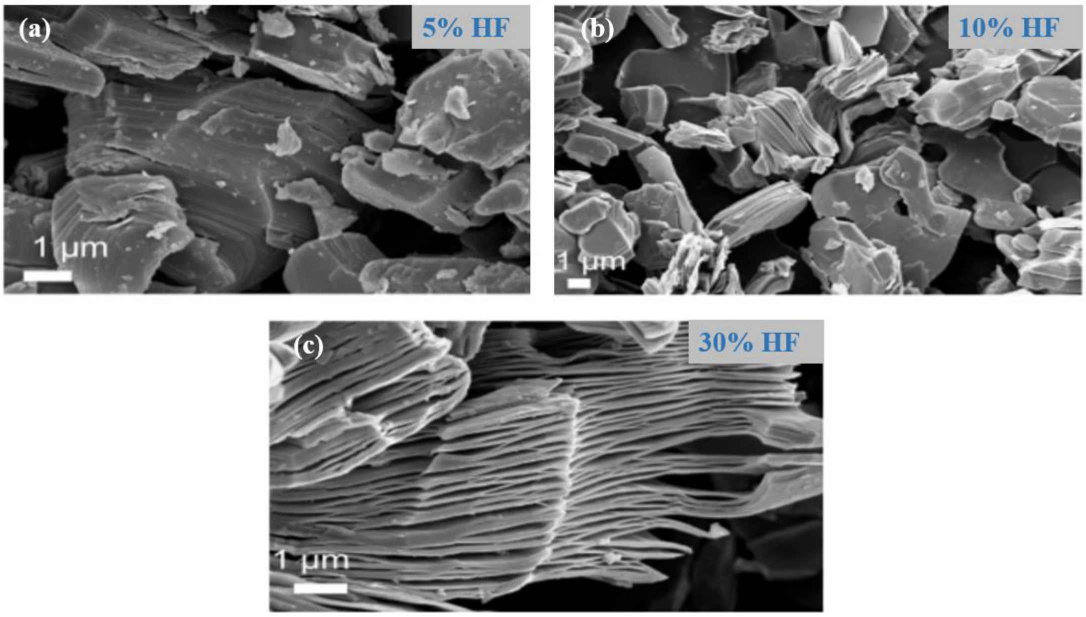

Figure 11: SEM images of MXene alloy etched with HF acid of different concentrations, (a) 5 % HF, (b) 10 % HF, (c) 30 % HF [19].

2.3.1.1 Top-Down Synthesis Methods

MXene nanosheets are typically made using the top-down synthesis approach. The method is based on the use of intercalants to separate the layers formed by etching of MAX precursor materials [20]. The schematic representation of the top-down synthesis method in general is given in Figure 12.

In the first step of MXene production, the bond between M and A 13tomsa re broken in the precursor MAX alloy ($M_{n+1}AX_n$) by selective etching. As an etchant, HF, NH_4F, NH_4HF_2, NaF, KF, HCl and LiF solutions are used [17-19].

During the etching process, the A atoms are eliminated. For example, by etching of Ti_3AlC_2 MAX alloy, Al is eliminated and $Ti_3C_2T_x$ Mxene alloy is obtained. In the resultant Mxene “T” represents -OH, -O, -F groups, which may vary depending of the etchant used. The control of surface groups in produced MXene is crucial since properties of the alloy depend on surface functional groups as well [21].

Etching methods applied to Ti_3AlC_2 MAX alloys are generally done under 60^{o}C temperature. On the other hand, synthesizing $Ti_3C_2T_x$ MXene from Ti_3AlC_2 MAX alloy using the hydrothermal methods requires higher temperatures, i.e., 270^{o} C, in NaOH solution [22]. As well as the carbide type MXene, various MAX alloys were also used for production of $Ti_4N_3T_x$ type MXenes. The first nitride MXene alloy $Ti_4N_3T_x$ was synthesized by heating Ti_4AlN_3 powders at 550 ° C under Ar gas using a mixture of molten salts, for example, LiF, NaF and KF [23].

A multi-layered accordion-like MXene structure is obtained just after etching process as seen in Figure 13. Additional exfoliation or intercalation are needed to produce a single-layer or few-layer MXene nanosheets. The etch procedure used and the composition of MXene determine the type of exfoliation technique [24]. MXenes are exfoliated using methods like sonication or shaking [25].

The intercalation process relies on increasing the d-space by placing organic molecules between the layers and separation of the layers by weakening the bonds even more. Generally, organic structures such as dimethyl sulphoxide (DMSO), TBAOH, TMAOH, urea are used [21-23]. The intercalation phase may not always be done. When LiF/HCl solution is used for MXene production, for example, Li cations settle between the layers and perform the intercalation step itself. Therefore, there is no need for an extra organic molecule for intercalation. After the intercalation process, the layers are exfoliated by sonication or shaking [25].

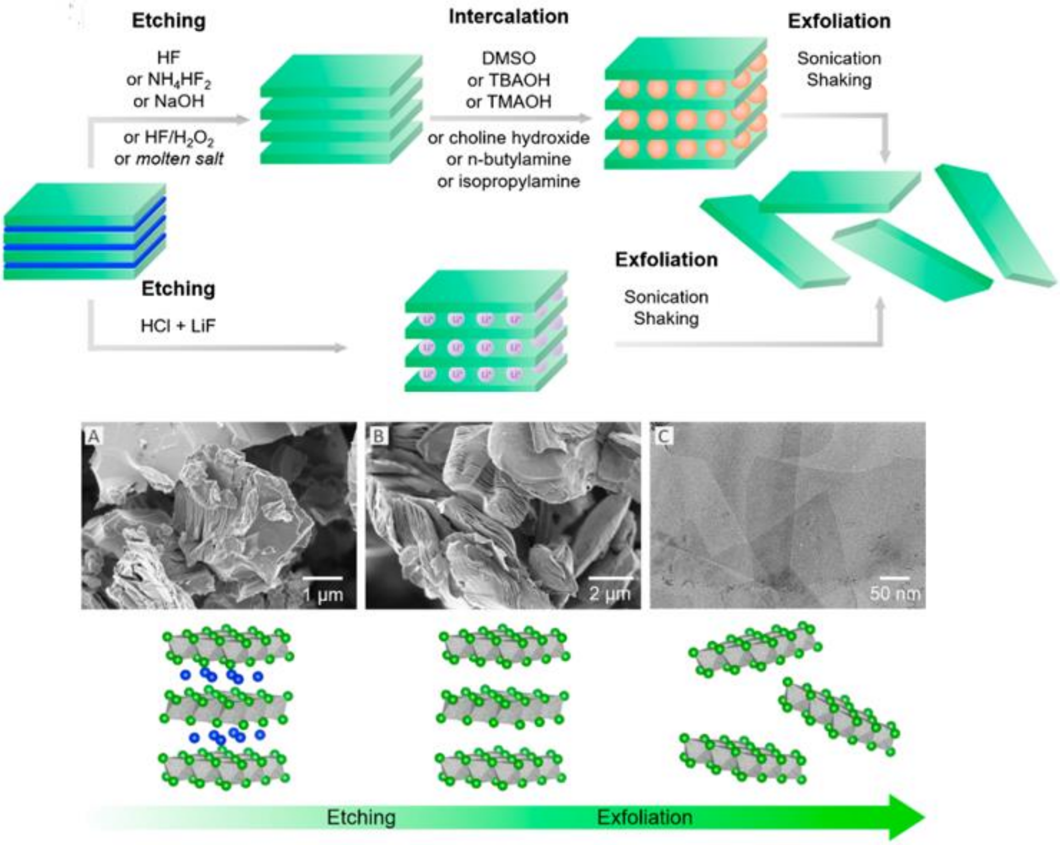

Figure 12: The schematic representation of the top-down synthesis method [26].

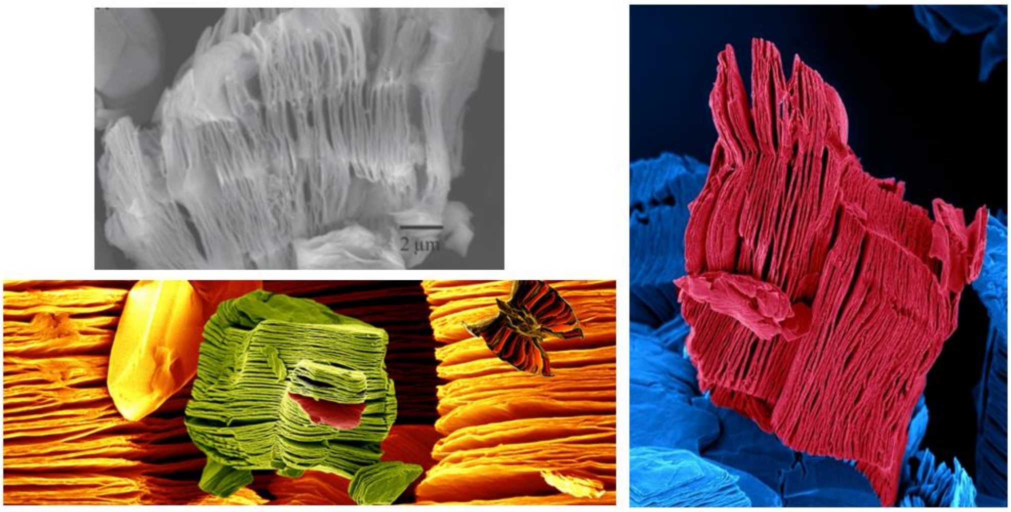

Figure 13: Colorless and colored SEM images of MXene alloys with layered structure obtained after etching [3].

2.3.2 Properties and Applications of MXenes

2.3.2.1 Electronic Properties and Applications

MXene alloys have high electrical conductivity, large specific surface area, and several redox zones. Due to these characteristics, it has shown that they are promising materials for energy storage, conversion, and supply applications. Boota et al. [27] observed that the MXene electrode had a greater capacitance density of 900 F cm^{-3} than other carbon electrodes in their research. Naguib et al. [16] used density functional theory (DFT) simulations to show that the MXene energy band gap varies with surface terminations (Figure 14). Ti_3C_2 without surface termination acts as a metallic conductor, but Ti_3C_2 alloys with surface terminations of -OH or -F behave like semiconductors. Because of their capacity to modify the bandgap, these materials may be employed in a wide range of applications, from field-effect transistors to semiconductors [16].

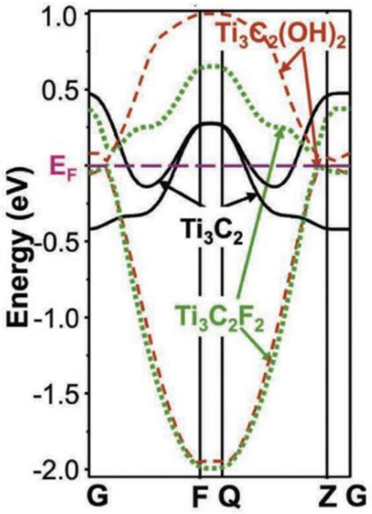

Figure 14: DFT calculations result of Ti_3C_2 with and without surface terminations of -OH and -F [16].

As they also have strong electrical conductivity and the capability of ions to spread easily across layers (Figure 15), MXene alloys have emerged as potential materials for lithium, sodium, aluminum, and potassium ion batteries. Li-ion and Na ion batteries have been the subject of studies to far [26].

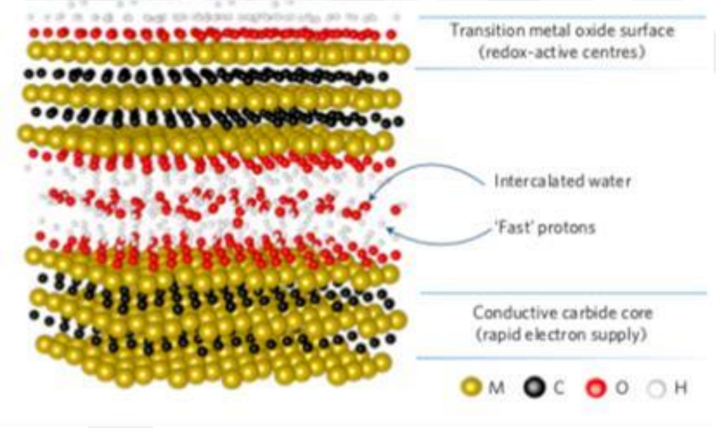

Figure 15: Charge storage mechanism of MXenes [28].

2.3.2.2 Optical Properties and Applications

One of the most noteworthy aspects noticed in previous investigations is the possibility of changing the optical properties of MXenes by altering the surface terminations. Simultaneously, it has been discovered that the optical characteristics of MXenes alter with the number of layers as well [29]. MXenes has extraordinary optical properties from UV to THz ranges so that MXenes could use various applications [30].

Additionally, studies have shown that MXenes have photothermal properties. MXenes with nanosheet structure turn into phonons due to the movement of photon energy in the lattice when the nanosheets absorb light [29]. It was observed that the released phonon energy significantly increased the temperature of the MXene nanolayer. In one of the studies [30], it was seen that $Ti_3C_2T_x$ absorbs sunlight to reach a temperature of 70 °C, and this feature can open a new way in biomedical applications, especially in anticancer treatment. The ability of MXene nanosheets reaching such a high temperature is enough to kill tumor cells and bacteria.

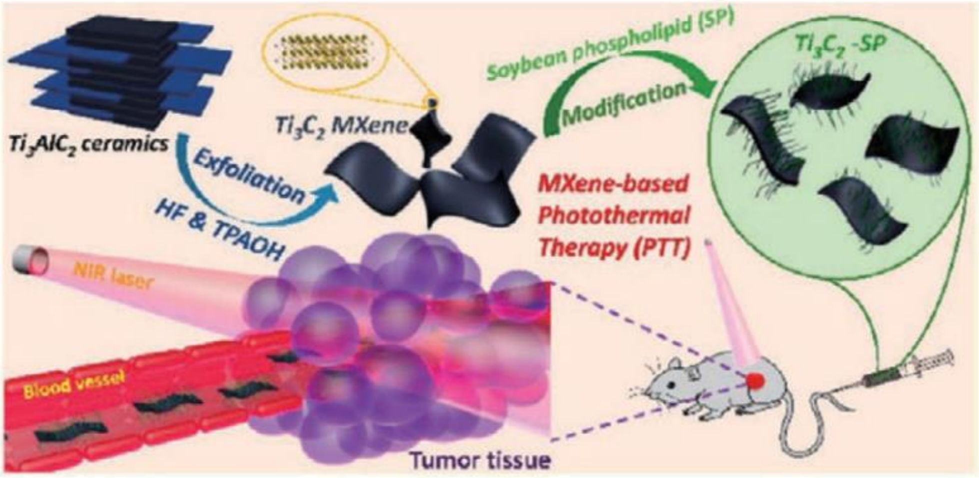

Figure 16: Schematics of photothermal effect of MXene for anticancer application [30].

2.3.2.3 Biomedical Properties and Applications

MXenes are frequently used in a wide range of biological applications, including drug administration, biosensing, medicine, bioimaging, and cancer treatment. The development of biosensors for in vitro and in vivo analyses requires a variety of special properties, including rich chemistry, optical absorbance, metallic conductivity, redox trait, excellent electron transfer capability, high hydrophilicity, and acceptable biocompatibility [31]. For instance, MXenes' properties significantly vary as a result of changes to their surface terminations brought about by interactions with various molecules (like various redox agents) [31,32]. They are suitable candidates for the creation of controlled MXene-based drug delivery systems due to their pH and near-infrared (NIR) responsive activity [33,34]. Furthermore, because of MXenes' strong photothermal conversion efficacy, they can eliminate cancerous cells through a combination of photothermal ablation and chemotherapy [33]. MXenes are used in a variety of biomedical applications, other than their antibacterial properties have attracted the most attention.

There is promising research for MXene to be used as a biomaterial to improve their biocompatibility by reducing cytotoxicity with their modified surfaces (Figure 17). Recent studies have shown that MXenes have great potential for drug delivery, antibacterial properties, tissue engineering and in Figure 18, examples of biomedical application areas where MXene alloys are used are given. [33].

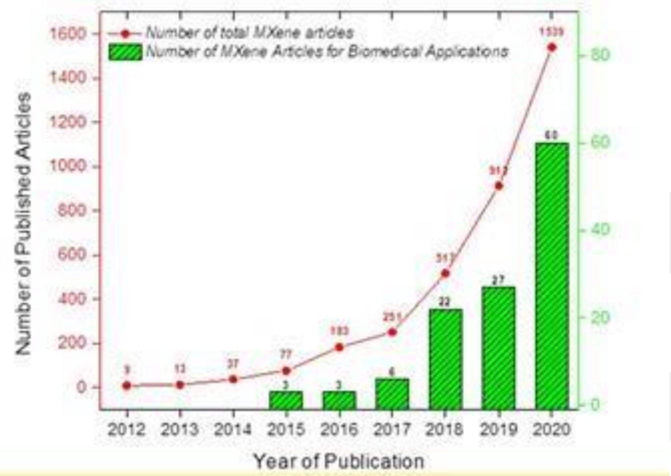

Figure 17: Number of MXene articles published about biomedical applications vs years [33].

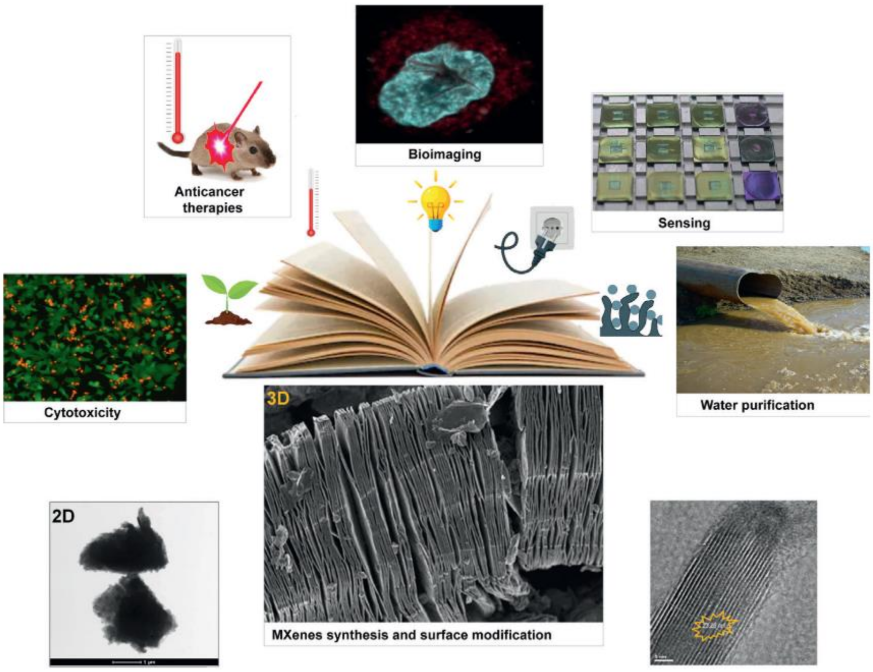

Figure 18: Examples of biomedical applications of MXene alloys [34].

2.3.2.3.1 Biosensors Applications

MXenes are excellent conductors of electricity such that one layer of them has a S/cm value of 4600 ± 1100. Due to its outstanding ion transport behavior and other good features, it is also extremely ideal to be used in biosensors which are effective instruments for finding both small and large biomolecules, as well as cancerous cells. It has been noted that several MXene composites, such as TiO_2-MXene or Au-MXene, are also produced in order to detect H_2O_2 and glucose [32].

Binghze et al. [32] made an ultrathin field effect transistor for probing neural activity using MXene. According to their findings, MXene displayed biocompatibility in sensitive biological systems and provided a good interface between neuron cells and electronic systems, allowing for label-free and real-time monitoring of neural spiking activities.

On the other hand, Liu et al. [33] created a 2D superparamagnetic composite made of Fe_3O_4 and MXene. They used these MXene composites for magnetic resonance imaging of tumors and as a powerful substance for destroying cancer cells.

2.3.2.3.2 Antibacterial Applications

The layered structure and sharp edges of MXene damage the membranes and disrupt the structure of the bacteria, and finally kills them. In addition, the oxides on the surface of MXene interact with the bacteria and break its structure. Therefore, MXenes are promising nanomaterials in the near future as an antibacterial biomaterial. Similar to graphene, MXenes have been shown to damage bacteria both physically and chemically [34,35]. Figure 19 shows schematically how this mechanism works. As seen in Figure 19, the sharp edges and surface of $Ti_3C_2T_x$ MXenes damage the walls of bacteria and destroy them.

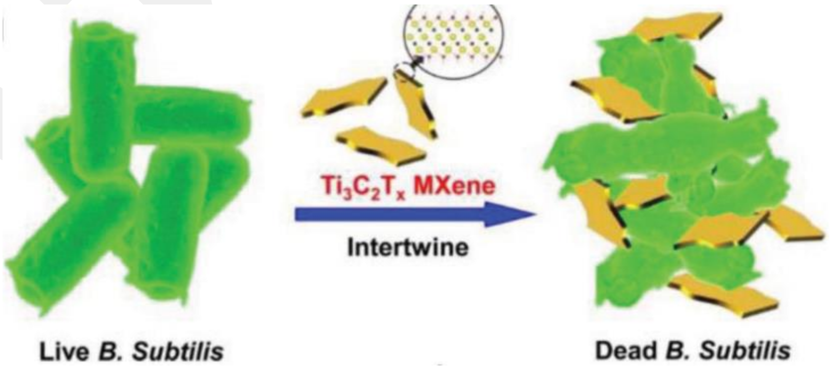

Figure 19: Schematically representation interactions between bacteria and MXene [34].

CHAPTER III

EXPERIMENTAL STUDY

3.1 RAW MATERIALS

Both commercial and the alloy powders produced in the present study are used for $Ti_3C_2T_x$ MXene alloy production. Elemental analysis of irregular shaped Ti_3AlC_2 MAX powders, supplied from Alfa Aesar, is shown in Table 2. The as received Ti_3AlC_2 MAX powders have 98 % purity.

For the production of Ti_3AlC_2 MAX alloy in the present study, TiH_2 (98% purity) powders (supplied Sigma Aldrich) were used as Ti source and mixed with aluminum powders (99,99 % purity) (supplied from Atlantic Equipment Engineers) and graphite powders were used as starting materials. The morphology and particle size distributions of the powders used are shown in Figure 20. In Table 3, the average particle sizes and size range of the powders are given.

Table 2: Elemental analysis of commercial Ti_3AlC_2 MAX powder

Element	**Wt. %**	**At. %**
Titanium	76.7	59.1
Aluminum	14.7	20.0
Carbon	5.4	16.5
Silicon	3.2	4.4

Table 3: Particle sizes of used powders for production of Ti_3AlC_2 MAX alloy.

Element	**Average Particle Size (µm)**	**Particle Size Range (µm)**
Ti_3AlC_2	19.5	8.7<…<46.4
TiH_2	8.6	3.9<…<12.3
Al	13.8	4.2<…<30.7
C	20.9	17.3<…<28.1

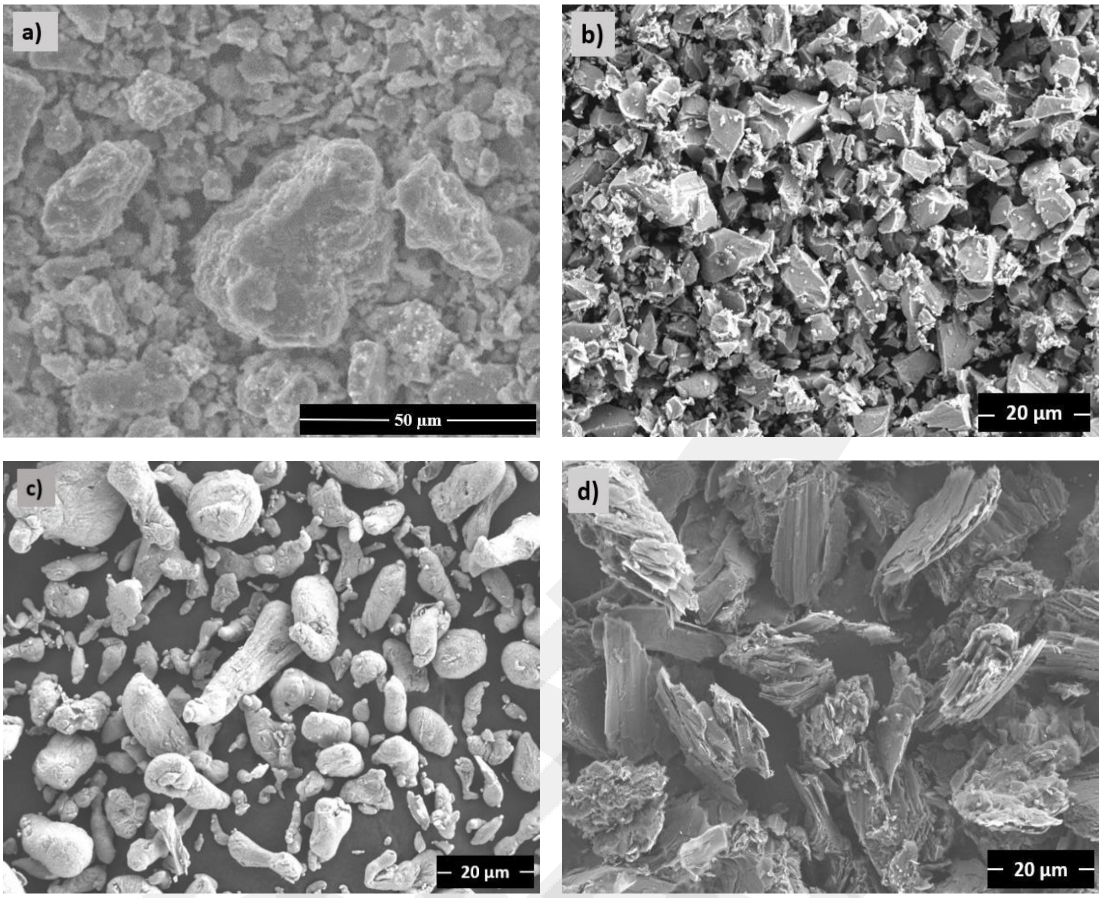

Figure 20: SEM images of a) Ti_3AlC_2, b) TiH_2, c) Aluminum, d) Graphite powders.

3.2 PRODUCTION OF Ti_3AlC_2 MAX ALLOY POWDERS

In addition to commercial Ti_3AlC_2 MAX alloy powders, the MAX alloy powders were also produced using powder metallurgy to investigate the effect of starting powders on $Ti_3C_2T_x$ MXene alloy production. Figure 21 summarizes the process used to synthesize Ti_3AlC_2 MAX alloy powders.

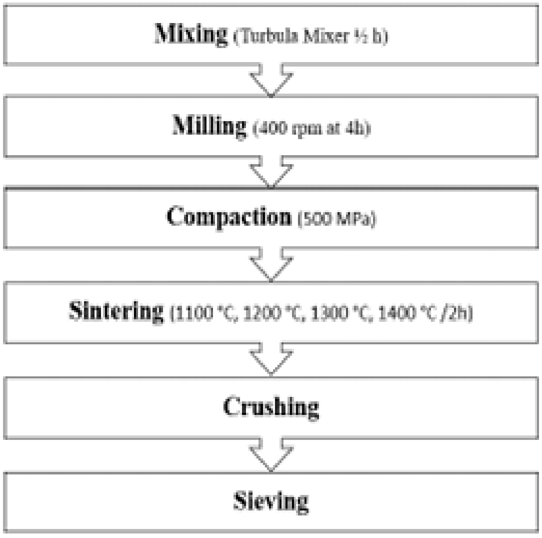

Figure 21: Schematic representation of Ti_3AlC_2 MAX alloy production route.

In order to produce Ti_3AlC_2 MAX alloy powders, firstly, TiH_2, Al and Graphite powders were mixed in ratio of 3:1:1 and totally 20 grams in a Turbula mixer for an hour. After initial mixing, the powders were milled using planetary ball mill (Retsch PM 100) in a zirconium container with a zirconium ball to powders ratio of 30:1 under high purity argon atmosphere at a speed of 400 rpm for 4 hours.

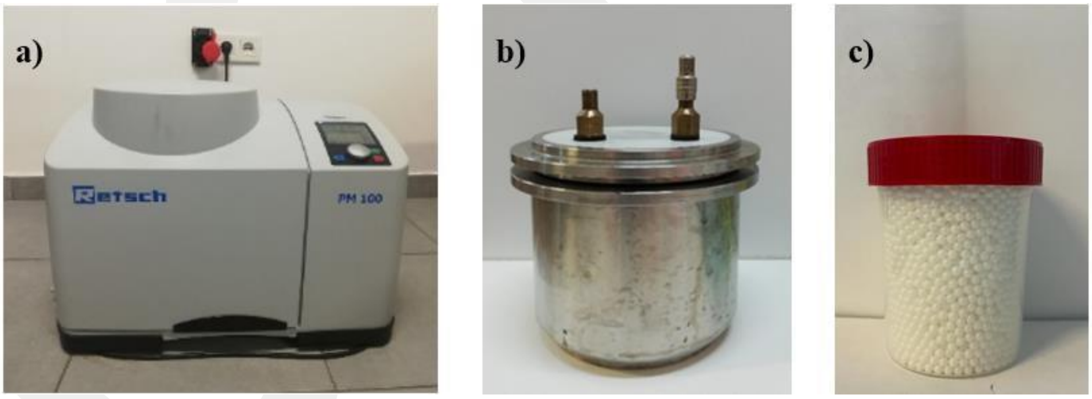

Figure 22: a) Retsch ball mill machine, b) Ball mill jar, c) Zirconia balls.

After obtaining the ball milled homogeneous powder mixture, the cold compaction of the powders was carried out at 500 MPa compaction pressure using a 10 mm diameter double-ended steel die. Afterwards, the obtained green compacts were placed in titanium alloy crucibles and put in the hot zone of an atmosphere-controlled horizontal tube furnace. In addition, titanium sponge particles (Ø 2-3 mm) were placed on the green compacts to prevent possible oxidation due to flowing argon gas (Ar >99.999%, O_2 <5 vpm, H_2O <4 vpm).

Before heating the tube furnace, air in the furnace was removed by a rotary type of vacuum pump and then, the furnace was re-filled with high purity argon gas which allowed to flow at least 3 min. through the furnace tube. Vacuum degassing argon purging cycles were repeated three times to ensure that the furnace was fully filled with Argon gas before starting the sintering process. Next, compacted powders were heated up to different sintering temperatures of 1100 ºC, 1200 ºC, 1300 ºC and 1400 ºC respectively, with a heating rate of 10 ºC/min. The samples were kept at the sintering different temperatures for 2 h and allowed to cool in the furnace after sintering.

After sintering process, the sintered samples were crushed in a marble mortar and sieved using 325-mesh sieve to obtain – 325 mesh Ti_3AlC_2 MAX powders.

3.3 SYNTHESIS OF $Ti_3C_2T_X$ MXENE ALLOY POWDERS

$Ti_3C_2T_x$ MXene powders were produced via the chemical etching method by using commercial Ti_3AlC_2 MAX powders and the MAX powders produced in the present study.

First of all, 50 mL eppendorf tubes, bullet used as a stirrer and 200 ml plastic sample cup were washed first with 1 M HCl and then with deionized water. Then, 20 ml of HF (38-40 %) was added to the plastic sample cup which was placed on the hot plate. The mixing speed was set to 300 rpm. Next, 1 gram of MAX powder (either commercial or laboratory produced) was added slowly in small amounts over 10 minutes. The MAX powder and acid solution were allowed to for 24 hours. The container was tightly closed to allow escaping of gasses produced during mixing. After etching, 20 ml of the prepared mixture was equally divided into two and 10 ml of mixture was added to 50 ml eppendorf tubes filled with 40 ml of deionized water. Afterwards, these tubes were placed in the centrifuge device (Elektro-mag M4800M) (Figure 23) at 3500 rpm for 5 minutes. After the centrifugation is finished, the pH of the solution was measured and then the supernatant was removed, and deionized water is added again. This process is repeated many times until the pH value reached to ~ 5. Finally, the settled powders in eppendorf tubes were taken to a glass container and dried under vacuum at 80 °C for 24 hours. Finally, dried MXene powders were kept in the freezer.

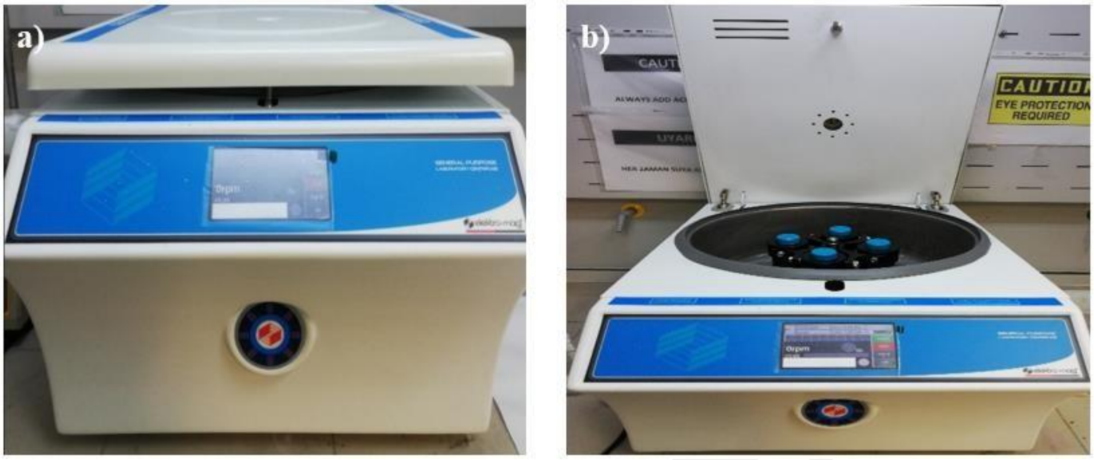

Figure 23: Elektro-mag laboratory centrifuge device.

3.4 COMPOSITE PRODUCTION

Polymer matrix composites containing PVA (5 %) and different amounts of MXene powders were produced to investigate the antibacterial properties. First, 5 % PVA solution was prepared by mixing solid PVA and deionized water at 80 °C for 2 hours. Then, MXene powder was added to PVA solution by 1, 5 and 10 wt. % and sonicated in an ultrasonic device for 2 hours at room temperature to produce composites. The prepared liquid phase composite was drop casted onto a 2 mm thick titanium bulk disc (99 % purity) and dried in an oven at 40°C for 24 hours under vacuum.

3.5 PRODUCTION OF MAX ALLOYS FOAMS

Carbamide was used as a space holder particle to produce MAX alloy foam. Around 70 vol. % carbamide powders with particle sizes between 300 and 500 micrometers were first added to Ti_3AlC_2 MAX alloy powders (Alfa Aesar) and hand mixed for ½ h. Then, the powder mixtures were cold pressed with double-ended steel die at 500 MPa. Afterwards, the green body was soaked in DI water at room temperature for 24 hours to remove carbamides by dissolution of it in DI water. Next, the green body, which was kept in an oven at 60 ºC for 2 hours for drying, was sintered under high purity argon at 1400 ºC for 1 hour.

3.6 PRODUCTION OF MXENE ALLOY FOAMS

The MXene alloy foams were produced by chemical etching of produced MAX alloy foams samples. MAX alloy foams initially were kept in HF for 24 hours at room temperature. Then, in order to remove the hydrofluoric acid, samples were washed several times with deionized water until the pH of the solution reached around 5.

3.7 ANTIBACTERIAL TESTS

Escherichia coli bacteria (gram negative) were reproduced in the METU Microbiology Laboratory in a petri dish at 37 ºC in an oven. Then, PVA coated on titanium disc (control group sample), MXene-PVA composites containing MXene around 1, 5 and 10 % by weight, which were coated on titanium discs previously, were smeared with E. coli bacteria. Afterwards, these samples were kept in a petri dish for one day in an oven kept at 37 ºC temperatures to observe bacterial growth. Antibacterial properties of the samples were determined by measuring the dead zone area (green region around the samples).

3.8 IN VITRO TEST OF SIMULATED BODY FLUID

Simulated body fluid (SBF), which mimics the composition of human plasma, is an in vitro test method to understand the biocompatibility or bioactivity of materials. If apatite formation is observed in the samples immersed in SBF, it can be said that the samples are biocompatible. In this study, samples were immersed and held in SBF for three different time periods to see the biocompatibility of MAX and MXene alloys foams.

In the first step, the preparation of SBF was placed in a polyethylene bottle with 700 mL of ion-exchanged deionized water at pH 8.2 and placed in a temperature controlled magnetic stirrer. Then the temperature was adjusted to 36.5 ± 0.5 °C degrees and the mixing speed was set to 300 rpm. Afterwards, as given in the Table 4 reagents were added, respectively, sodium chloride (NaCl), sodium hydrogen carbonate ($NaHCO_3$), potassium chloride (KCl), di-potassium hydrogen phosphate trihydrate ($K_2HPO_4.\ 3H_2O$), magnesium chloride hexahydrate ($MgCl_2.\ 6H_2O$), HCl, calcium chloride ($CaCl_2$) and sodium sulfate (Na_2SO_4). Here, care was taken to add $CaCl_2$ slowly and in small amounts several times in order to dissolve $CaCl_2$ completely. After all the reagents were dissolved, 900 mL of deionized water was added, and the pH was 2.0 ± 1.0 and the temperature was 36.5 ± 0.5 °C. Then, Tris was added slowly and in small amounts each time so that the pH did not suddenly increase. The process continued until the pH reached 7.40 at 36.5 ± 0.5 °C degrees. When the final temperature 36.5 ± 0.5 °C and pH remained at 7.4, the solution was made up to 1000 mL with deionized water. The prepared SBF was cooled to room temperature and then put in the refrigerator to wait at 5 ºC-10 ºC degrees.

In order to examine the apatite formation in the MAX and MXene alloys foams, the samples were maintained in the SBF at 36.5 ± 0.5 °C degrees for 1, 5, 15 and 25 days, respectively. To maintain a steady ion concentration throughout the test, the SBF solution was changed every two days. The samples were withdrawn from the SBF after keeping them for predetermined time and then cleaned with deionized water. Finally, all samples were kept at room temperature for 24 h for drying.

Table 4: Simulated body fluid reagents and their relative amounts.

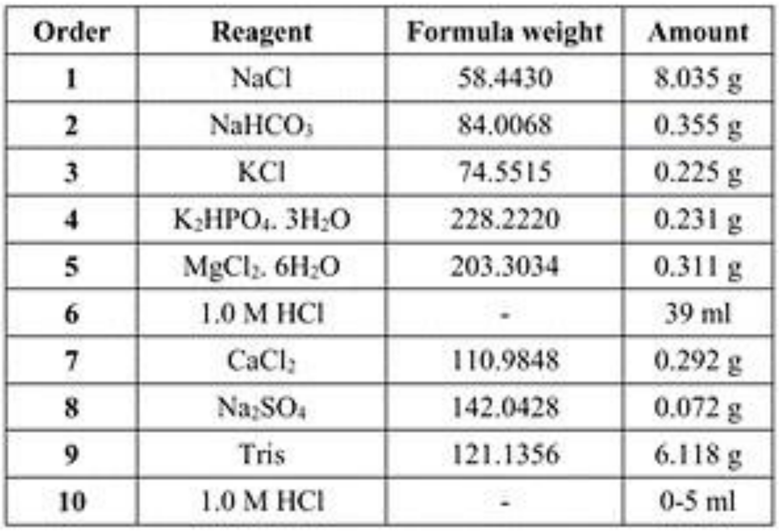

Order	Reagent	Formula weight	Amount
1	NaCl	58.4430	8.035 g
2	$NaHCO_3$	84.0068	0.355 g
3	KCl	74.5515	0.225 g
4	K_2HPO_4. $3H_2O$	228.2220	0.231 g
5	$MgCl_2$. $6H_2O$	203.3034	0.311 g
6	1.0 M HCl	-	39 ml
7	$CaCl_2$	110.9848	0.292 g
8	Na_2SO_4	142.0428	0.072 g
9	Tris	121.1356	6.118 g
10	1.0 M HCl	-	0-5 ml

3.9 CHARACTERIZATION TECHNIQUES

3.9.1 Microstructural Analysis

Morphological and microstructural examination of sintered compacts, powder forms, and foams of Ti_3AlC_2 MAX alloy, and the synthesized $Ti_3C_2T_x$ MXene alloy powders and $Ti_3C_2T_x$ MXene alloy foams were performed by “FEI 430 Nano Scanning Electron Microscopy” (SEM) equipped with an energy dispersive X-Ray spectroscopy (EDS) analyzer. Compact Ti_3AlC_2 alloy samples produced in the study after sintering were also examined in the etched condition after grinding and polishing the surfaces using SiC papers 220-2000 grit size and diamond (3-0,25) suspended solution, respectively. The etch solution was composed of HF, HNO_3 and H_2O (% vol. 1:1:1).

3.9.2 Structural Analysis by X-Ray Diffraction Analysis (XRD)

X-Ray diffraction analysis was performed to examine the phases formed in the produced samples. "Bruker D8 Advance Eco model X-Ray Diffractometer" and "Rigaku D/Max 2200/PC, Rigaku Corporation, Tokyo, Japan" instruments were used for structural analysis. Ti_3AlC_2 MAX alloy scanned with Cu-Kα radiation continuously between 10° and 80° 2ϴ angles at a scan speed of 1° /min. On the other hand, $Ti_3C_2T_x$ MXene alloy powders scanned between 5° and 80° 2ϴ angles at scan speed of 1° /min.

3.9.3 X-Ray Photoelectron Microscopy (XPS)

XPS analysis was performed to understand the surface chemistry of starting Ti_3AlC_2 MAX alloy powders and $Ti_3C_2T_x$ MXene powders. The X-Ray photoelectron spectroscopy (PHI 5000 VersaProbe) device, which uses monochromatised Al radiation, was used for analysis. (Al mono 48.1 W, 200.0 MM, 187.85 eV). Powder samples were examined by general surface scanning and resultant binding energy calibration was done by taking the energy position of C 1s in hydrocarbon CH2 (284.6 eV) as reference.

3.9.4 Particle Size Analysis

Ti_3AlC_2, TiH_2, aluminum and graphite powders were investigated using the ImageJ program on images taken with a "FEI 430 Nano Scanning Electron Microscope" (SEM) in order to estimate particle sizes.

CHAPTER IV
RESULTS AND DISCUSSIONS

This chapter consists of three main parts about production of Ti_3AlC_2 MAX alloy and synthesis of $Ti_3C_2T_x$ MXene alloy using MAX alloy, and characterization of both alloys including structural, image, surface and elemental analyzes. The functional properties of the produce alloys were also determined via application of in vitro simulated body fluid and antibacterial tests.

4.1 PRODUCTION OF Ti_3AlC_2 ALLOY POWDER

4.1.1 Ball Milling of Starting Powders

MAX alloys play a significant role in the synthesis of MXenes as they serve as precursors. The purity and lack of contamination of MAX alloys are critical for the synthesis of MXene.

The type and purity of starting materials play a crucial role in the production of Ti_3AlC_2 MAX alloy. In the powder metallurgical processes, in most cases, pure Ti or TiH_2 powders are used as titanium source, while graphite, TiC, or carbon lampblack was preferred as carbon source. It was discovered that use of different carbon and titanium sources altered the structure of resultant $Ti_3C_2T_x$ MXene, which was synthesized form Ti_3AlC_2 MAX alloy [36]. In this study, as described previously, TiH_2 was employed as a source of Ti during production via powder metallurgy since the resultant sintered compact has a porous structure which enabled crushing of Ti_3AlC_2 MAX alloys easier for production of alloy powders. On the other hand, high purity graphite powders were used due to ease of supply.

In the first part of the study, prior to $Ti_3C_2T_x$ MXene alloy synthesis, various optimization studies were carried out to produce high purity Ti_3AlC_2 MAX alloy via powder metallurgical method. Therefore, initially mechanical alloying parameters were optimized prior to MAX alloy production. As mentioned in experimental studies section, firstly, TiH_2, Al, and C powders were mixed in a zirconium jar using zirconium balls. The ball mill speed and time are important parameters for efficient production mixing and alloying. According to previous works, two different speeds (400 and 600 rpm) and time (1 and 3 hours) were selected. As can be seen in Figure 24, high speed milling at 600 rpm for 1 and 3 hours didn’t produce any Ti_3AlC_2 MAX alloy. In contrast, milling at 600 rpm resulted in severe oxidation of Al powders and induced formation of Al_2O_3 phase together with TiC. Additionally, as can be seen EDS analysis (Figure 22), Zr element was also detected in addition to Ti, Al, O and C elements as a result of milling at 600 rpm. High speed milling probably caused microcracking of ball mill jar and ball; thereby, resulting contamination of milled powders. Accordingly, ball milling speed was reduced to 400 rpm, and, at the same time, the time was increased to 4 hours to ensure effective milling. Decreasing the ball milling speed eliminated Zr element in ball milled powders (Figure 25(c)). Although the oxidation of powders was not eliminated completely, comparatively low amount of Al_2O_3 phase was detected, Ti_3AlC_2 MAX alloy formation was detected as well together with TiC (Figure 24). Therefore, before the sintering process all powders were milled at 400 rpm for 4 hrs under a high purity argon atmosphere. As can be seen in Figure 26, the powders were mostly agglomerated, and the size of the milled powders were observed to change between submicron size and 100 µm.

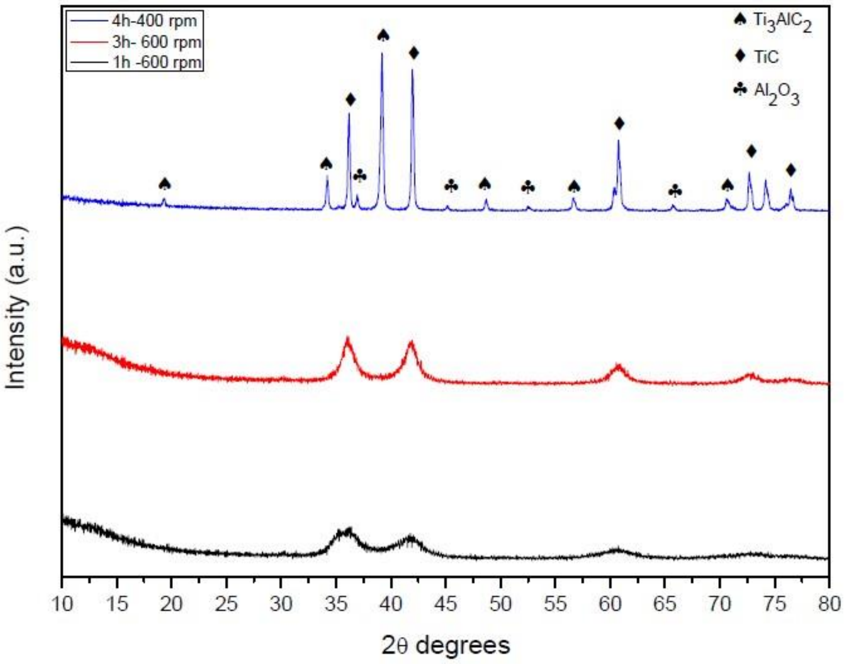

Figure 24 : XRD patterns of ball milled powders.

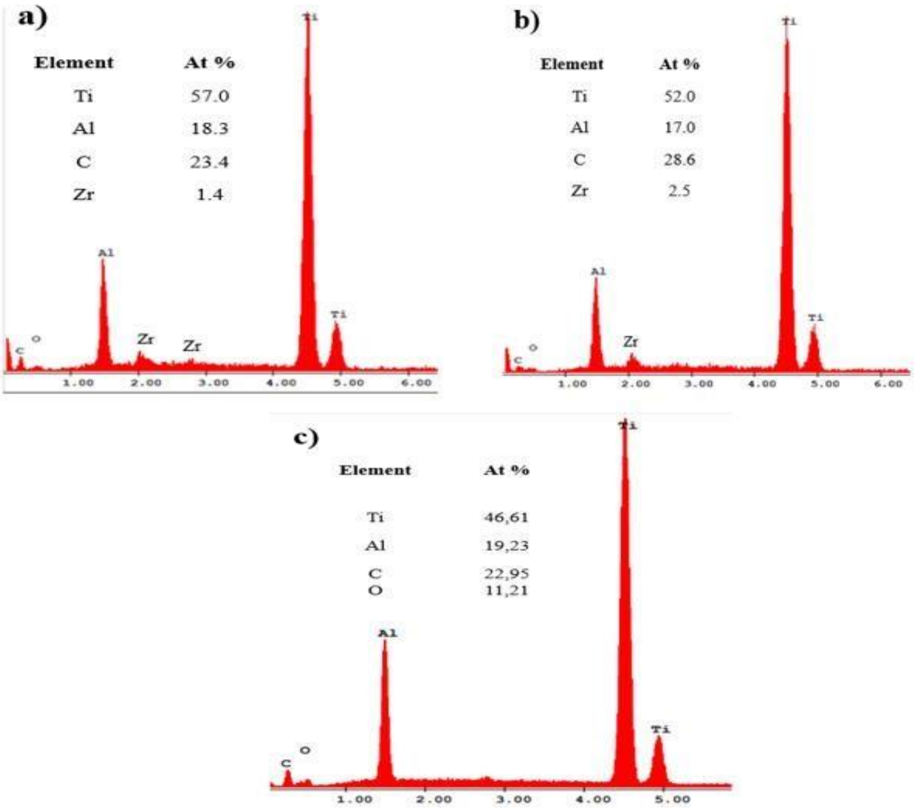

Figure 25: EDS analysis of powders ball milled for (a) 1 hour at 600 rpm, (b) 3 hours at 600 rpm and, (c) 4 hours at 400 rpm.

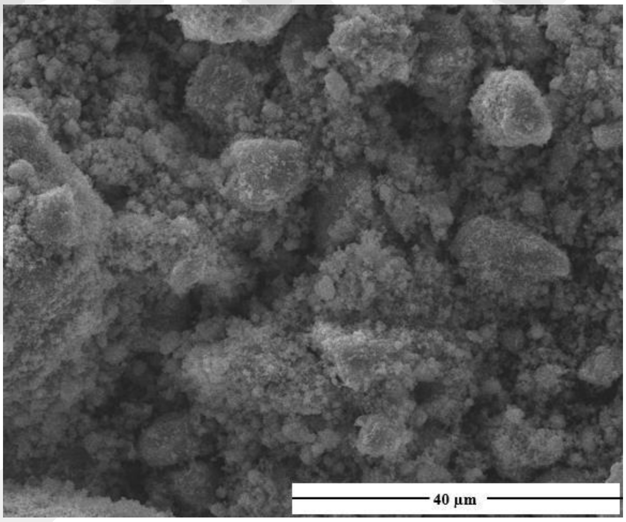

Figure 26: Powders milled at 400 rpm for 4 hrs.

4.1.2 Sintering and MAX Alloy Powder Production

In the powder Ti_3AlC_2 MAX alloy powder production step, initially, cold pressed powders, milled at 400 rpm for 4 hours, are sintered at various temperatures for 2 hours with the aim of mixing and mechanical alloying. Next, the powders were cold compacted at various temperatures for 2 hours to ensure Ti_3AlC_2 phase formation.

Table 5 displays the average density and total porosity of sintered compact at different temperatures. The presence of porosity in the samples makes powder production easier since crushing becomes easier. As expected, the samples' density increases as sintering temperature increases. The porous structures of sintered compacts are presented in Figure 27.

Although sintering between 1100 °C and 1300 °C resulted in porosity, the sample sintered at 1400 °C had almost no porosity. In terms powder production, it is usually better to choose porous structures; however, the quantity of Ti_3AlC_2 phase is the most important criteria in determination of proper sintering temperature. As can be seen in Figure 28, sintering up to 1300 °C caused formation of considerable amount of TiC phase in addition to Ti_3AlC_2. On the other hand, upon sintering at 1400 °C, the samples contained mostly Ti_3AlC_2 phase with slight amount of TiC phase. Microstructural investigation of the sample revealed plate like and round phases with similar chemical composition close to Ti_3AlC_2 phase (Figure 29). Therefore, samples sintered at 1400 °C were selected for Ti_3AlC_2 powder production.

Table 5: Density and Porosity of sintered powders at various temperatures and time.

Sintering Temperature, T (°C)	**Sintering Time, t (hour)**	**Average Density, ρ (g/cm^3)**	**Total Porosity, P (%)**
1100	2	3.2	24.5
1200	2	3.5	17.5
1300	2	3.9	8.0
1400	2	~ 4.24	~ 0

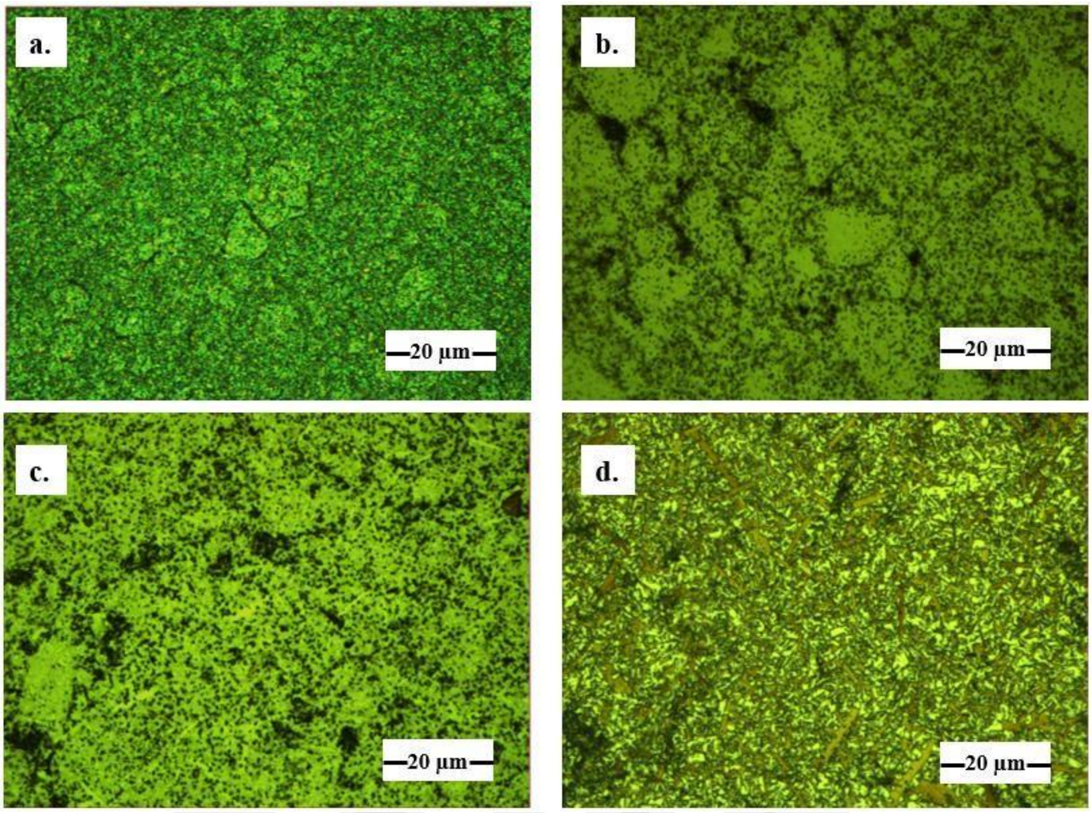

Figure 27: Optical images of sintered powders at (a) 1100 °C, (b) 1200 °C, (c) 1300 °C, (d) 1400 °C

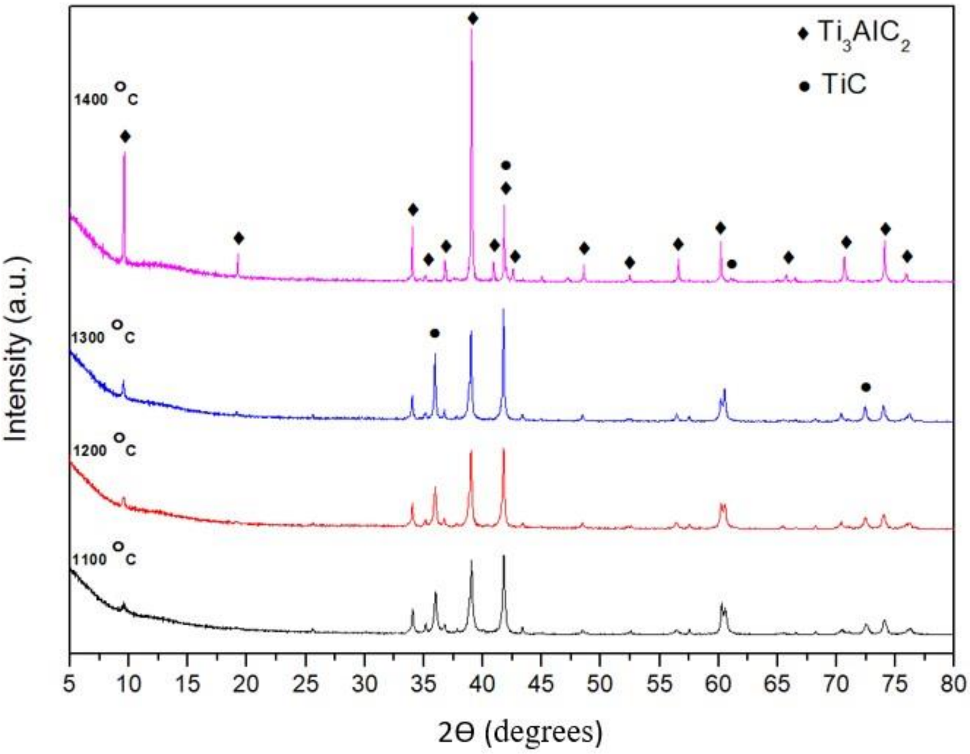

Figure 28: X-Ray diffraction patterns of samples sintered at different temperatures.

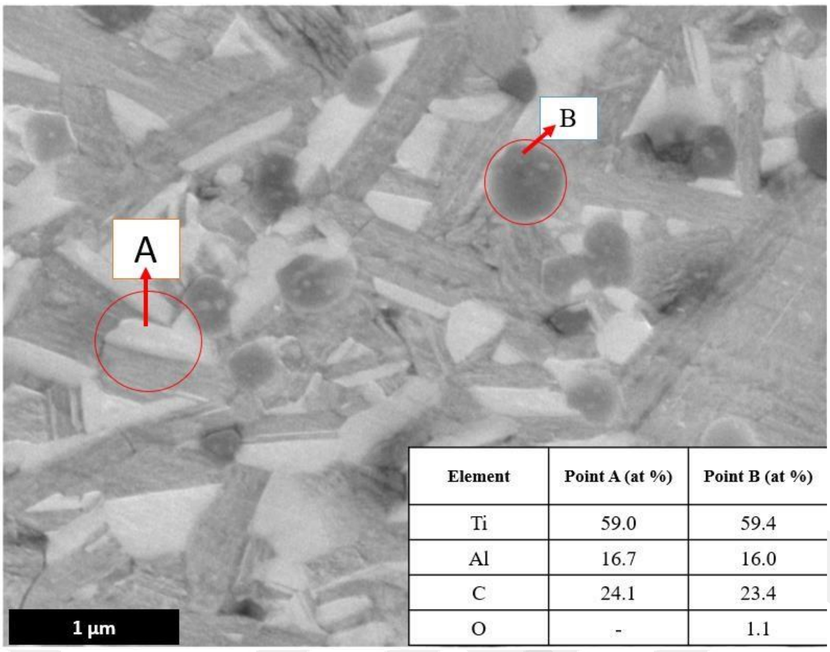

Element	Point A (at %)	Point B (at %)
Ti	59.0	59.4
Al	16.7	16.0
C	24.1	23.4
O	-	1.1

Figure 29: SEM graph of sample sintered 1400 °C and the corresponding EDS analysis of points A and B.

Figure 30 shows the structure and EDS analysis of powders produced from compacts sintered at 1400 ^oC. After crushing the compacts using agate mortar sieving was applied using 325-mesh sieve. The size of the powders was below 45 µm and they were mostly round in shape.

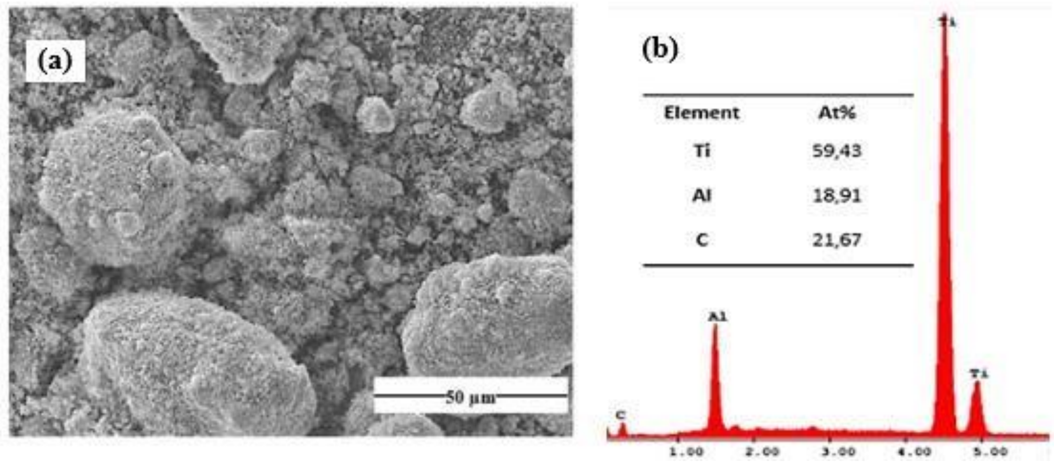

Element	At%
Ti	59,43
Al	18,91
C	21,67

Figure 30: (a) SEM image and, (b) EDS analysis of powders produced from the compacts sintered at 1400 °C for 2h sintered sample.

4.2 SYNTHESIS OF $Ti_3C_2T_X$ MXENE

In this study, $Ti_3C_2T_X$ MXene alloy was synthesized from commercial (supplied from Alfa Aesar) and laboratory produced Ti_3AlC_2 MAX alloy using the selective wet etching process in which HF acid is used for etching of Al sites in the alloy [37]. The weak van der waals bonds between Ti and Al are broken to create the $Ti_3C_2T_X$ alloy according to equations (1)-(3) as described below [38].

$$Ti_3AlC_2(s) + 3\ H^+(aq) \rightarrow Ti_3C_2(s) + Al_3^+(aq) + 3/2\ H_2(g) \quad (1)$$

$$Al_3^+(aq) + 3\ F^-(aq) \rightarrow AlF_3(aq) \text{ and } Al_3^+(aq) + 6\ F^-(aq) \rightarrow AlF_6^{\ 3-}(aq) \quad (2)$$

$$Ti_3AlC_2(s) \rightarrow Ti_3C_2(s) + 3\ e^- + Al_3^+ \quad (3)$$

In order to obtain high purity MXene alloy Al based ions were effectively removed by centrifugation several times using DI water until the pH of the solution reached 5. After removal excess solution, $Ti_3C_2T_X$ MXene powder was obtained upon drying the sediment that settled to the bottom of the containers. Figure 31 shows the morphology of commercial, and laboratory produced powder after being etching process. As can be seen, round starting commercial MAX powders with 15.0 µm particle size, (Figure 31(a)) turned into flower-like structure and its size decreased to 7.7 µm, Figures 31 (a) and (b) as a result of etching Al selectively. The relative amount of Al element in the alloy reduced down to ~1.9 at. % (Figure 31(c)). Although the relative amount of Al in etched laboratory produced MAX alloy ~3.3 at. %, similar flower-like morphology is not obtained. The etching of lab produced alloy significantly reduced to powder particle size from 1.8 µm to 0.9 µm and plate like structures were rarely observed. Probably the surface properties of laboratory produced alloy resulted in different etching response. Therefore, the experiments continued with commercial MAX alloy since flower-like morphology was not obtained although various etching procedures were applied to laboratory produced MAX alloy.

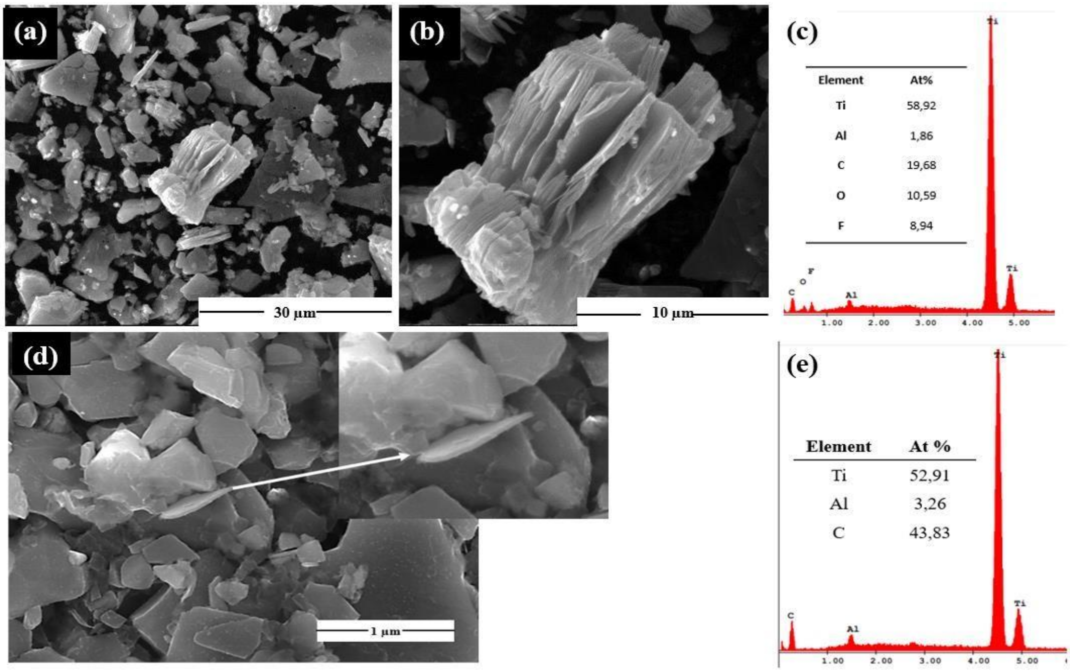

(c)

Element	At%
Ti	58,92
Al	1,86
C	19,68
O	10,59
F	8,94

(e)

Element	At %
Ti	52,91
Al	3,26
C	43,83

Figure 31: SEM images of (a), (b) $Ti_3C_2T_x$ MXene synthesized from commercial Ti_3AlC_2 MAX alloy powder and, (d) $Ti_3C_2T_x$ MXene synthesized from lab produced Ti_3AlC_2 MAX alloy powder and, EDS analysis of (c) $Ti_3C_2T_x$ MXene synthesized from commercial Ti_3AlC_2 MAX alloy powder, (e) $Ti_3C_2T_x$ synthesized from laboratory produced Ti_3AlC_2 powder.

To decrease the Al content and to obtain the few layers of MXene sheets, produced MXene alloy were sonicated. Sonication produced clearer flower-like structure; however, no plate-like structures were obtained (Figures 32 (a) and (b)). More powerful sonication techniques like probe sonication is needed to synthesize single layer MXene alloy. On the other hand, additional sonication was effective in decreasing the Al content by eliminating excess etched Al encapsulated between layers. As can be seen in EDS analysis, Figures 31(c) and 32(c), sonication increased the relative oxygen content of the MXene alloy.

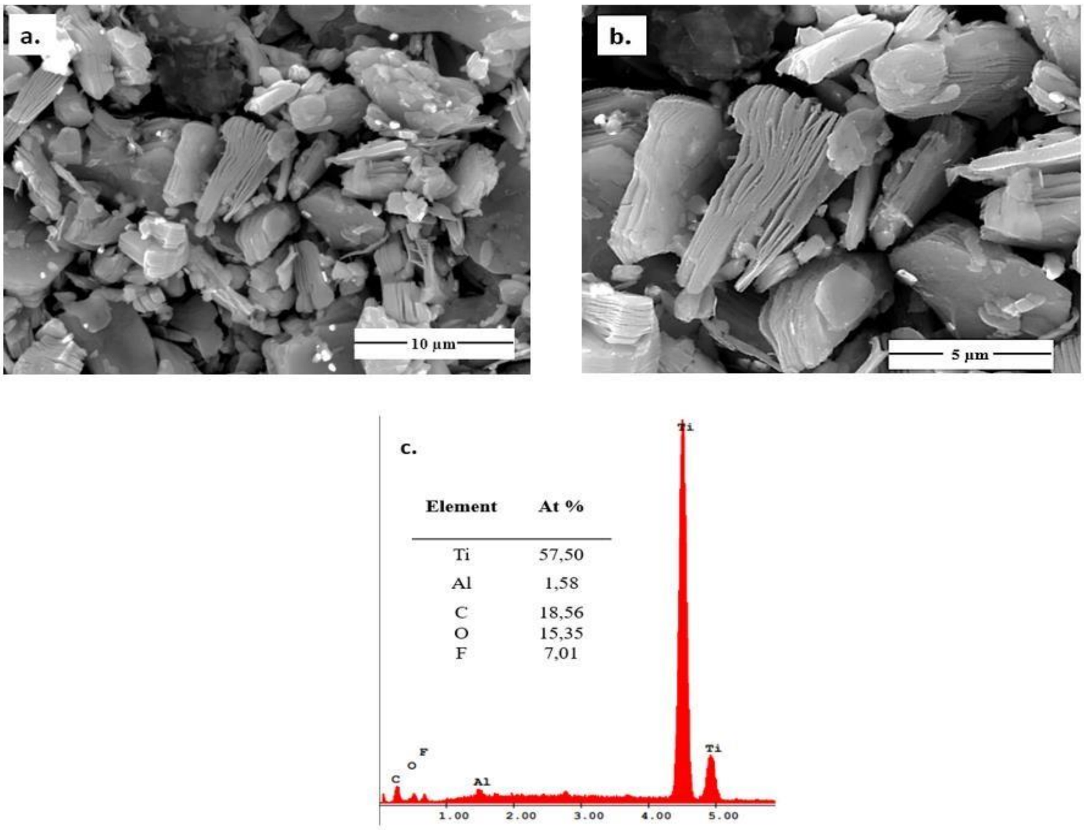

Figure 32: SEM images of sonicated MXene alloy and its EDS result.

Figures 33 and 34 display the XRD results of MXene alloy powders synthesized using commercial MAX alloy powder at their as produced and sonicated condition. As can be seen, etching of the commercial MAX alloy resulted in complete transformation of Ti_3AlC_2 to $Ti_3C_2T_x$ phase. The characteristic peaks of Ti_3AlC_2 at 2ϴ angles of 39° and 42° had disappeared and Ti_3C_2Tx MXene formation was observed. Moreover, etching removed all TiC phase in the MAX alloy. On the other hand, sonication of the powders with deionized water for 1 hour in the ultrasonic device after etching to obtain single layer MXene caused additional TiO_2 phase formation as seen at around 2ϴ angle of 25° in Figure 34. The presence of TiO_2 phase was also detected in microstructural examination in the form of white particles (Figures 32 (a) and (b)). Possibly, keeping MXene alloy in aqueous solution for prolonged times results in severe oxidation of MXene layers. Accordingly, sonication for single layer MXene layer formation was excluded.

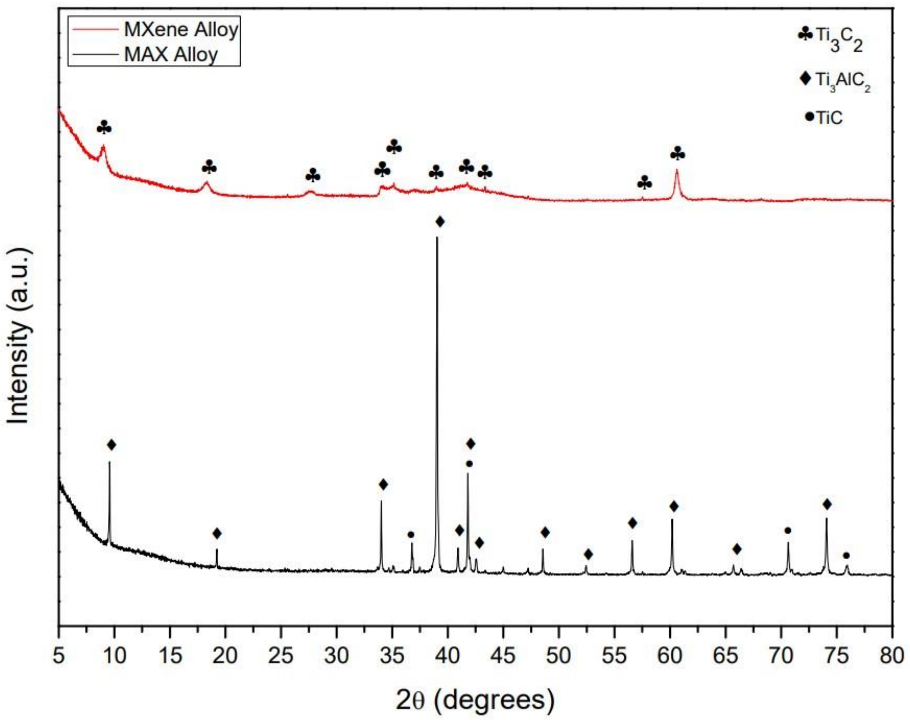

Figure 33: XRD patterns of commercial Ti_3AlC_2 MAX powders and MXene alloy powders produced from the commercial MAX alloy powders.

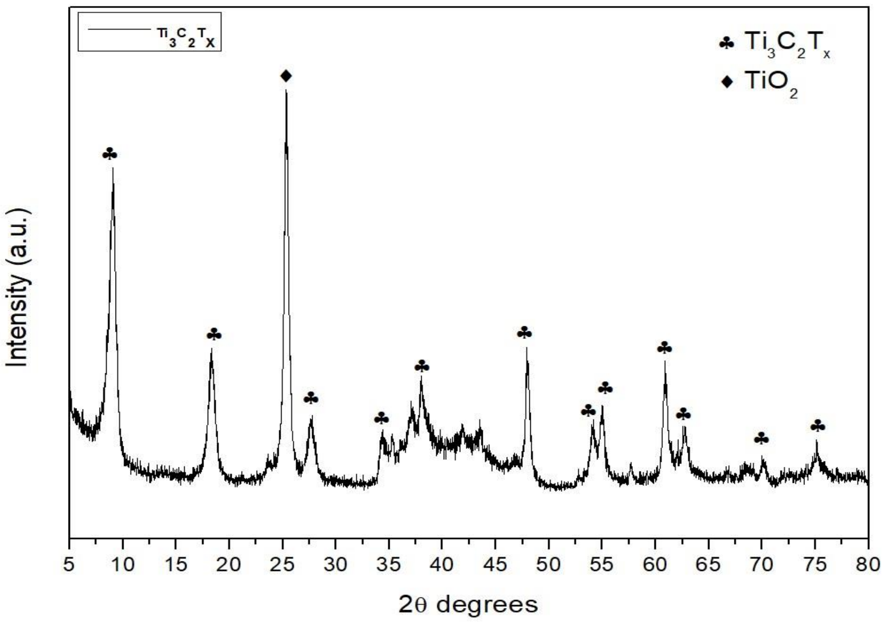

Figure 34: XRD patterns of MXene alloy sonicated for one hour.

In $Ti_3C_2T_x$ MXene alloy, T represents termination groups. It is known that MXene alloy sheets produced by etching with HF acids are terminated with oxygen- and/or fluorine-containing functional groups (=O, -OH, -F). Although elimination of sonication prevented additional oxidation of MXene, synthesized MXene sheet surfaces contained as much oxygen as in the starting MAX alloy as can be seen in XPS spectra (Figures 35(a) and (b)). Moreover, the presence of F element can also be clearly seen which is the indication of formation –F functional groups.

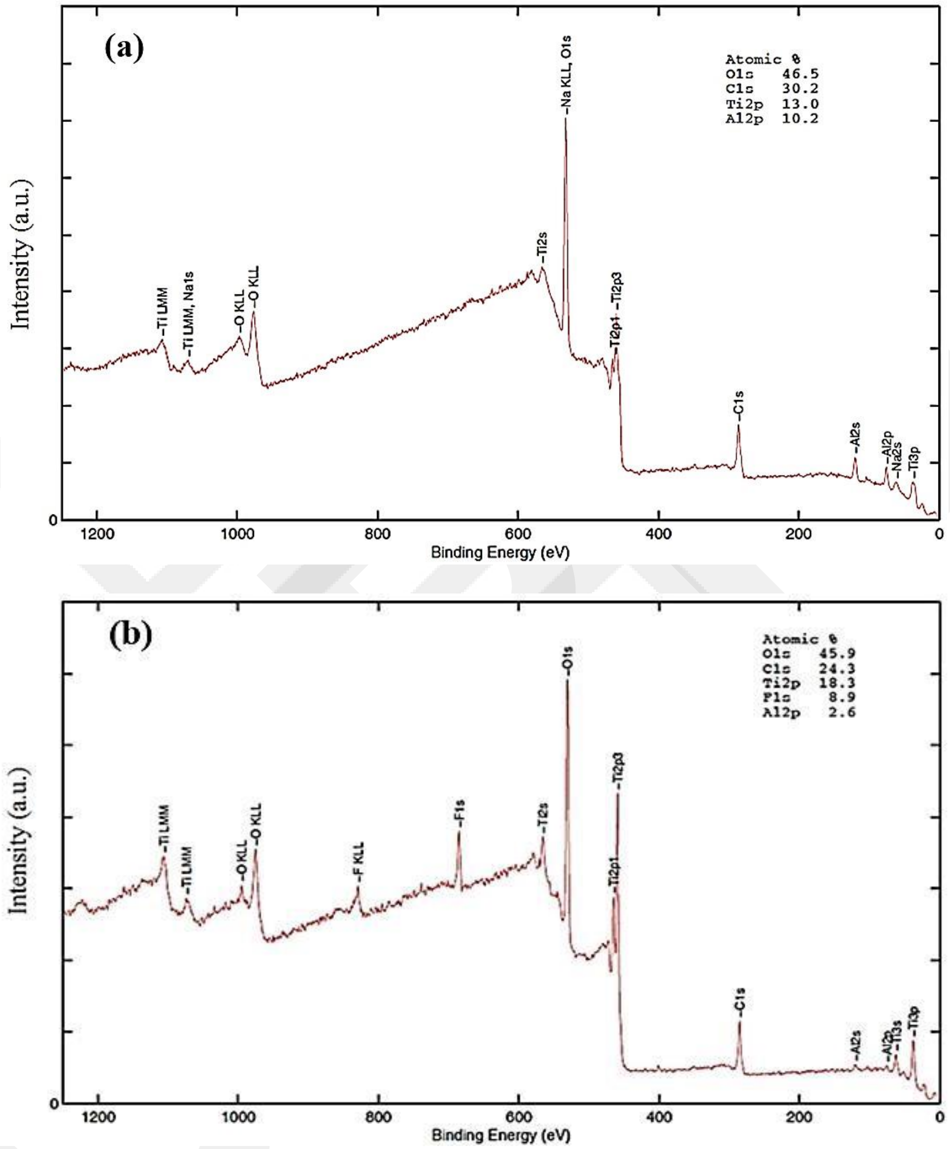

Figure 35: XPS results of (a) As-received commercial MAX alloy, (b) Synthesized MXene alloy using MAX alloy.

4.3 PRODUCTION OF FOAM SAMPLES

4.3.1 Ti_3AlC_2 MAX Alloy Foams

As mentioned in the experimental section, commercial Ti_3AlC_2 MAX powders were mixed with carbamide spacer particles to create porosity around 70 % after evaporation of carbamide upon heating for sintering. However, sintered compacts' porosity was measured to be around 46% mainly due to excessive shrinkage during sintering. Likewise, the size of the macro pores, obtained upon evaporation of carbamide particles, were around 407 µm, which was smaller than the starting carbamide size of 500 µm due to sintering shrinkage. As can be seen in Figure 36, MAX alloy foams contained interconnected macro pores and micro pores due to partial sintering on the call walls. Interconnection of the pores is crucial in biomedical application in which body fluid transfer plays an important role for ingrowth of bone tissues.

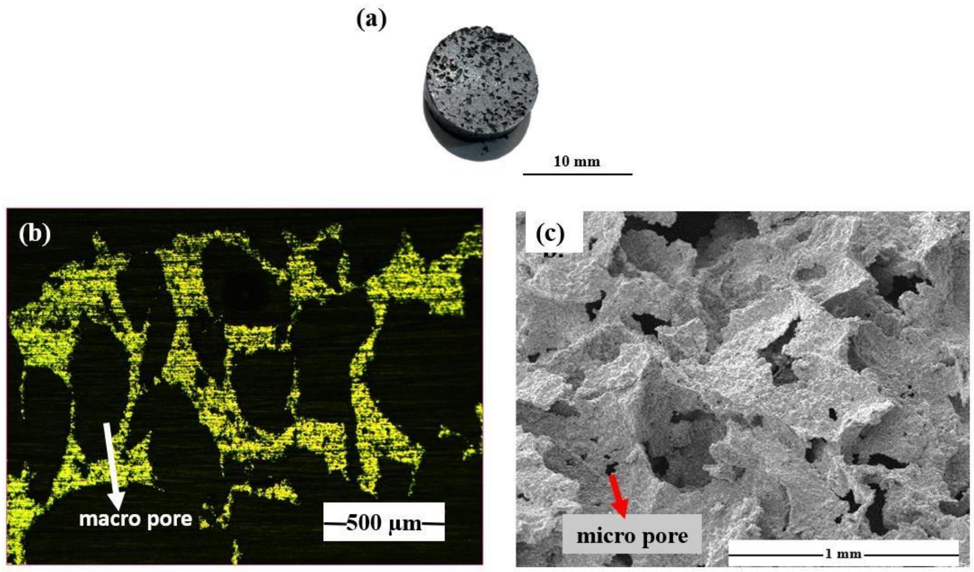

Figure 36: (a) Macro image of porous MAX alloy, (b) Optical microscopy image taken from the cross-section of porous MAX alloy and, (c) SEM image of porous MAX alloy.

A three-dimensional image of cell wall structures is given Figure 37 with the corresponding EDS analysis. Microporous cell walls with partially sintered powders contained Ti, Al and C elements as expected; however, Si element was detected as some regions which was believed to come from starting powders. As can be seen Figure 38, Ti_3AlC_2 MAX alloy foam produced from commercial powder also contained TiC phase in addition to Ti_3AlC_2 phase as detected in the as-received powder (Figure 33). TiC peaks seen at 2Θ angles of 34^{o}, 71^{o} and 76^{o} in as-received powders' XRD pattern disappeared and TiC phase was detected only at 62^{o} as a shallow peak. This result indicates that sintering the starting powder for foam production caused more Ti_3AlC_2 phase formation by consuming TiC in the powders, which aids maximizing the MAX phase.

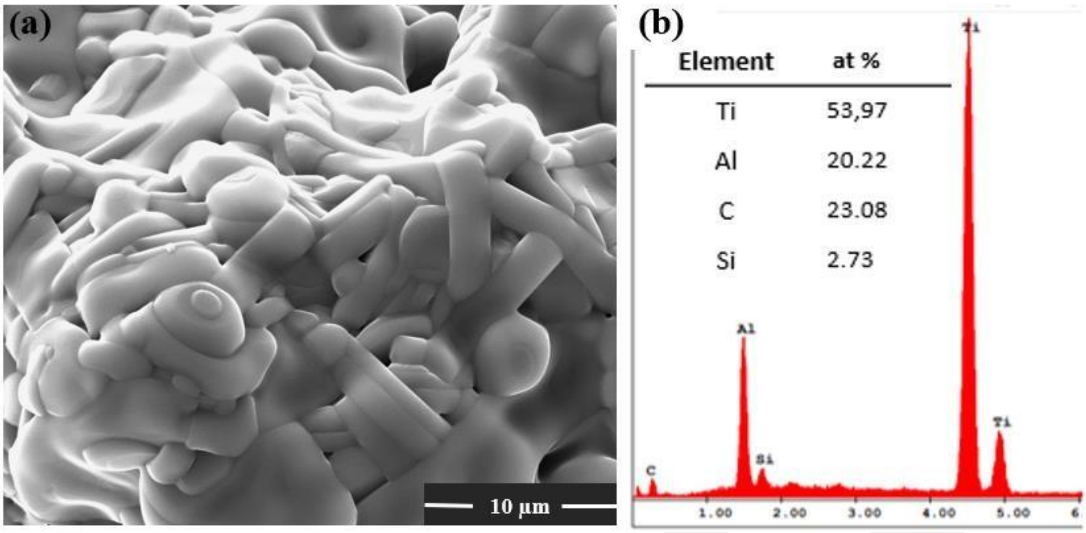

Element	at %
Ti	53,97
Al	20.22
C	23.08
Si	2.73

Figure 37: MAX alloy foam produced from commercial powder (a) SEM image, (b) corresponding EDS analysis.

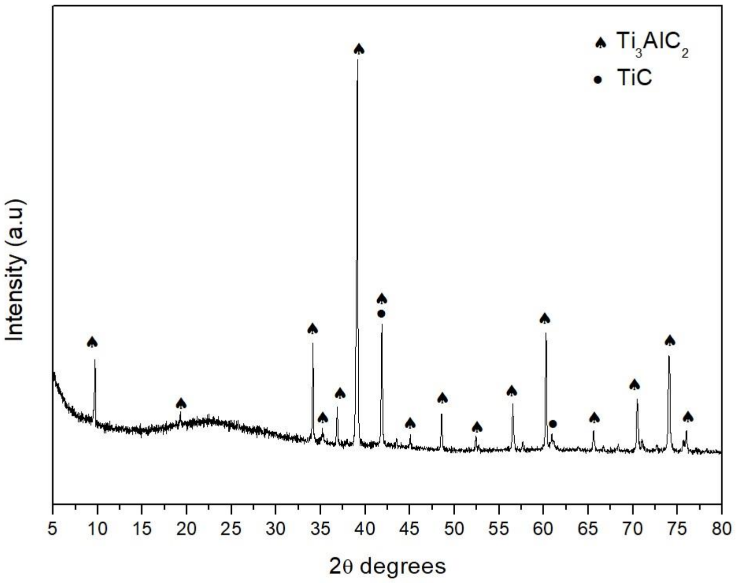

Figure 38: XRD pattern of MAX alloy foam produced from commercial powder.

4.3.2 Production of $Ti_3C_2T_x$ MXene Alloy Foams

$Ti_3C_2T_x$ MXene alloy foams were produced from commercial Ti_3AlC_2 MAX alloy foams using HF etching previously used for MXene powder production. To the best of authors' knowledge, no work was done on the production of MXene alloy foams. The current study aimed at production and functional characterization of MXene alloy foams for biomedical applications.

MXene alloy foams produced by keeping MAX alloy foams in HF acid for 24 hours showed no disintegration and there was no obvious color change as observed in MXene powder production stage.

Figure 39 shows macro and micro image of produced MXene foams. Similar to MAX alloy foam, the samples were composed macro pores with around 400 µm average pore size, which didn't change too much as a result of etching. In addition, cell walls of the foam samples contained micro pores due to partial sintering.

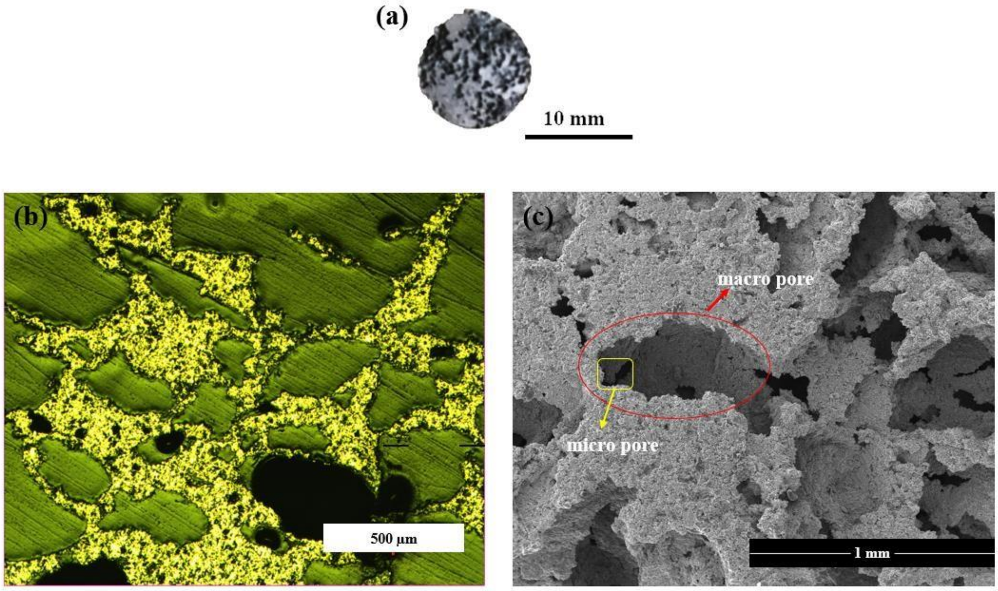

Figure 39: (a) Macro image of MXene alloy foam, (b) Optical image taken from the cross-section of MXene alloy foam and, (c) SEM image of MXene alloy foam.

SEM image of cell walls given in Figures 40 (a) and (b) clearly shows flower like structures in the partially sintered powders because of Al etching. However, not all the regions of the alloy seperated into layers and comperatively higher Al content (4.6 at. %) was observed with respected MXene powders (1.9 at. % Al) produced using the same etching technique. Possibly, reduced surface area by partial sintering the MAX powders decreased the etching efficiency of HF acid. On the other hand, similar to powder MXene, F element was detected.

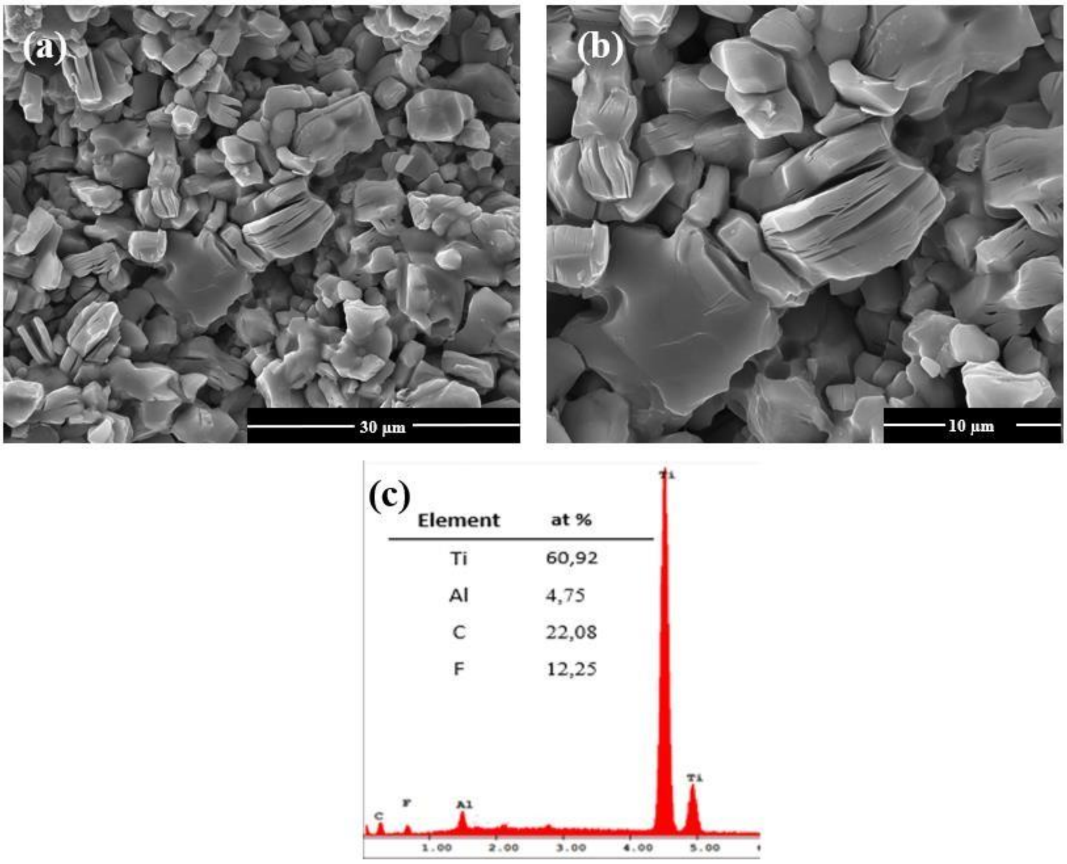

Figure 40: SEM images and EDS result of foam MXene alloy at different magnifications.

Figure 41 shows the XRD patterns of MAX and MXene alloy foams. Although the SEM image (Figure 40(b)) shows formation of flower like structures clearly, no $Ti_3C_2T_x$ phase was detected possibly due to its low amount. On the other hand, Ti_3AlC_2 and TiC phases seen in MAX alloy foams were still present in MXene alloy foams.

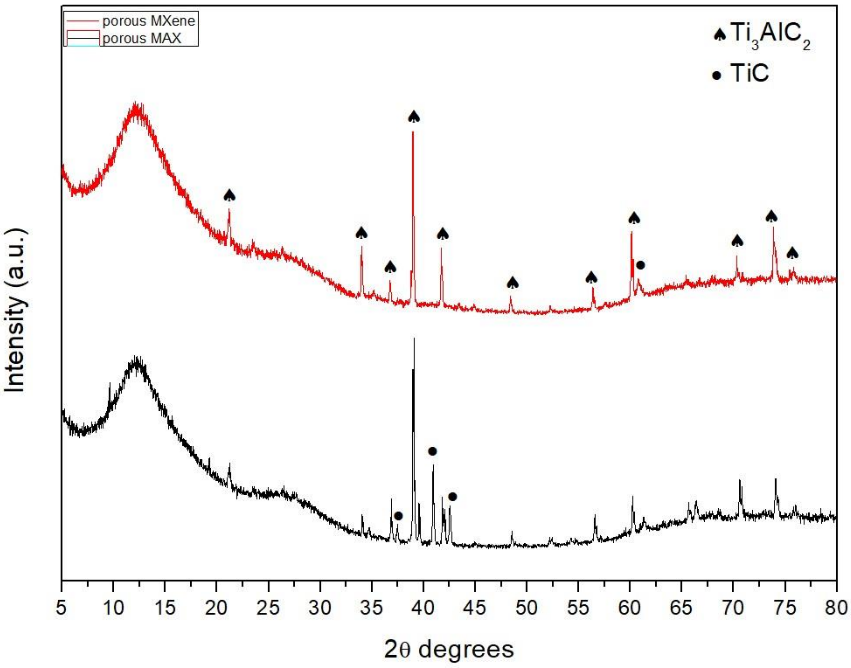

Figure 41: XRD patterns of MAX and MXene alloy foams.

4.4 SIMULATED BODY FLUID TESTS

MAX and MXene alloy foam samples were kept in SBF at 36,5 ± 0,5 °C for various times (1, 5, 15 and 25 days) to investigate the relative apatite formation abilities.

Figure 42 shows the XRD patterns of MAX and MXene alloy foams kept in SBF for various times. For both samples, there were no clear apatite peaks up to 25 days immersion except Ti_3AlC_2 and TiC phases observed in the starting foam samples.

Closer examination of cell walls revealed hemispherical apatite like structures in MAX alloy foam after 15 days (Figure 43), which covered most of the cell walls. On the other hand, very small white precipitates were detected in MXene alloy foams after one day, however, they didn’t grow even after 25 days. Since the precipitated phases in both types of alloy foams covered the internal regions of the foams, they were not detected in XRD patterns.

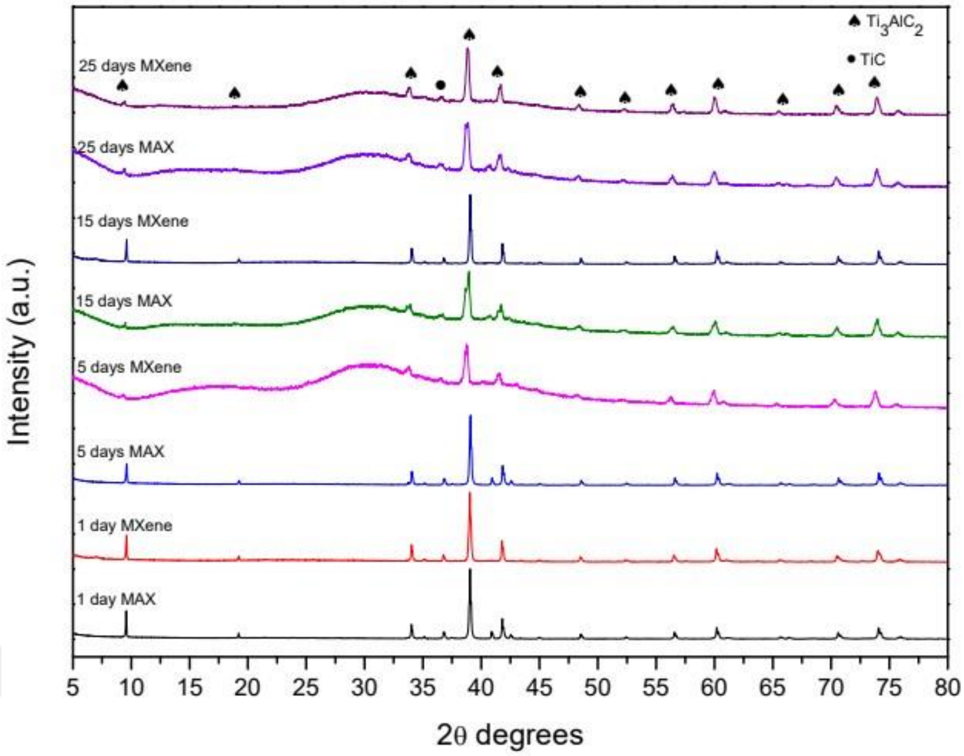

Figure 42: XRD patterns of MAX and MXene alloy foams kept in SBF for various times.

Biological apatite found in bone and synthetic hydroxyapatite both primarily comprise Ca and P elements, with Ca/P atomic ratios of 1.655 and 1.667 in each form of apatite, respectively, Table 6 shows the change in Ca and P elements quantity and their ratio for different soaking time in SBF. The EDS analysis taken from the rarely observed white precipitates in MXene alloys revealed P deficient Ca precipitation for the first 5 days. The first P precipitation observed after 15 days; however, Ca/P ratio was too high (2.4) for apatite. The ratio of Ca and P in MXene alloy foams became around 1.8, close to ratio found in apatite, after 25 days. But the precipitates were still observed rarely on cell walls of foams. Although there was no precipitation in MAX alloy foams in the first 5 days, Ca/P ratio got close (1.5) to apatite in the precipitated phases after 15 days, which showed that the precipitated phase was apatite. The Ca/P ratio became 1.6 after 25 days as well. Based on the SBF tests, MAX alloy foams exhibited better apatite formation ability compared to MXene alloy foams. Despite the rougher cell wall cell of MXene alloy less Ca and P precipitation occurred possibly due to presence of fluorene-based termination groups in $Ti_3C_2T_x$ formed during etching by HF acid.

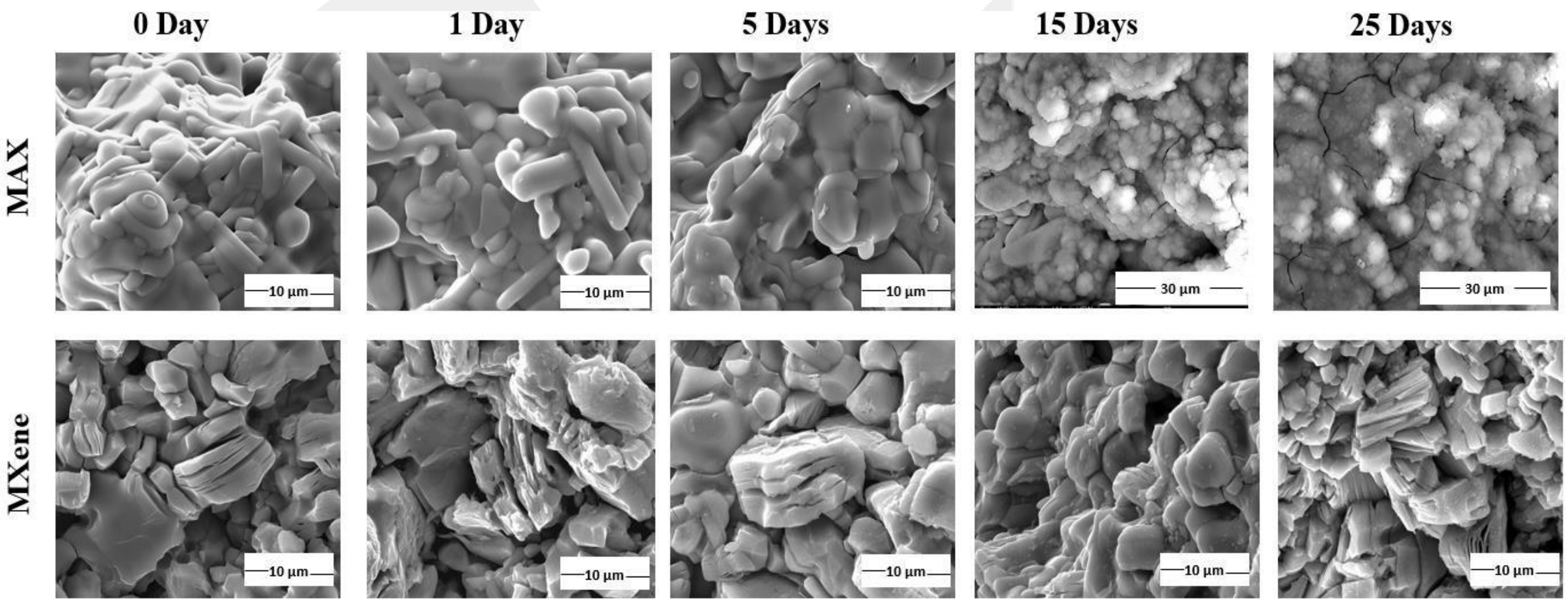

Figure 43: SEM images of MAX and MXene alloy foam samples immersed in SBF for 0, 1, 5, 15 and, 25 days.

Table 6: Ca/P ratio of porous MAX and MXene samples immersed in SBF 1, 5, 15 and, 25 days.

Element	at. %							
	1 day immersion		5 days immersion		15 days immersion		25 days immersion	
	MAX	MXene	MAX	MXene	MAX	MXene	MAX	MXene
Ca	-	1.0	-	1.4	26.9	2.0	36.6	2.2
P	-	-	-	-	18.4	0.80	23.2	1.2
Ca/P	-	-	-	-	1.5	2.4	1.6	1.8

4.5 ANTIBACTERIAL TESTS

Escherichia coli (E. coli) gram negative bacteria is one of the most common causes of many common bacterial infections in humans and animals. The therapeutic treatment of E. coli infections is threatened by the emergence of antibacterial resistance. This, unfortunately, causes an increased rate of diseases caused by drug resistant E. coli bacteria. Therefore, it is important to treat E. coli bacteria, which has become increasingly resistant to antibiotics, with different methods. $Ti_3C_2T_x$ MXene alloy has a reputation for destroying bacteria due to its sharp layers that are directly contact with bacteria [39]. Zone of Inhibition Test, also called a Kirby-Bauer Test, which is mostly based on macro-observation, was used for antibacterial tests in this study. According to this method, bacteria are grown on agar, then it is checked whether a visible zone is formed around the sample to be tested or not. If a zone is formed, it means that the bacteria are dead, and the material displays antibacterial properties [40].

In this study, MXene alloy powders were tested by mixing them in PVA, a biodegradable polymer. Next, the PVA-MAX and PVA-MXene composites coated on Titanium discs which were used as substrate material for the composite. It is clearly seen from Figure 44 that the produced MXene alloy has antibacterial properties. In addition, when PVA and MXene alloy are used together to form a composite, the antibacterial properties of the composite increase when the quantity of MXene increases as revealed by the green area (dead bacteria) around the samples.

In addition, when looking at other composites, it is seen that zones forms around them and as the MXene composition increases, the zone also increases. In Figure 45, the graph of MXene composition and zone ratio is given. Looking at this graph, it is seen that 1 wt. % MXene-PVA composite is less resistant to E. coli bacteria than the composites containing MXene by 5 and 10 wt. %, which showed bacterial resistance close to each other.

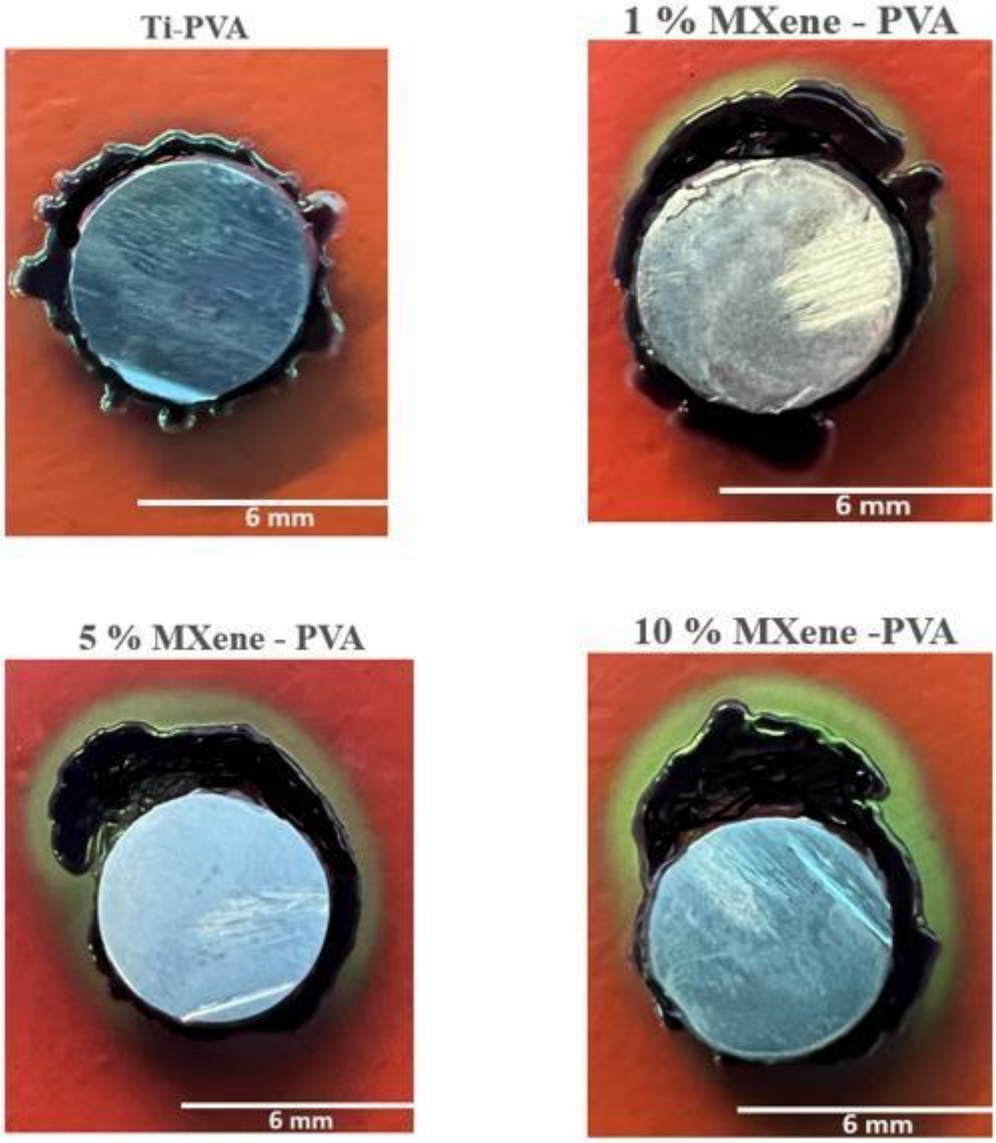

Figure 44: Zone of inhibition test results of composites containing MXene in different compositions (wt. %) placed on an agar plate with E. coli bacteria.

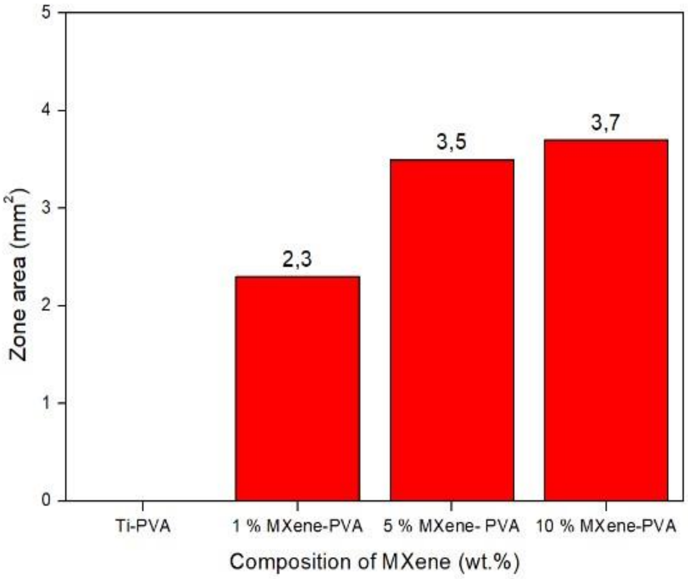

Figure 45: The graph of compositions of composite (in wt. %) and zone ratio.

CHAPTER V
CONCLUSIONS

In the present study, following conclusions can be drawn about the production and characterization of powder and foam counterparts of MAX and MXene alloys:

1- Although commercial Ti_3AlC_2 MAX alloy powders contained TiC and Ti_3AlC_2 phases, produced MAX alloy powders, obtained via grinding of MAX alloy compacts sintered at 1400 ^oC, displayed very low amount of TiC phase.

2- Ball milling of sintered MAX alloy compacts at 400 rpm for 4 hours was considered to be optimum since ball milling at higher speed for longer times caused contamination with ZrO_2, which came from the fractured zirconia balls and the jar.

3- Etching of commercial and lab produced MAX alloy powders by HF acid decreased the average powder particles size and Al content of both powders significantly; however, Al couldn’t be removed completely.

4- Flower like multilayered MXene powders were obtained via chemical etching, while no layered structure was observed in lab produced alloy despite decreased Al content.

5- Sonication method, which was applied for obtaining layered MXene structure with thinner MXene plates and for removing the Al residue in the solution, caused remarkable oxidation of the powders.

6- PVA-MXene composites displayed antibacterial properties and higher antibacterial resistance to Escherichia coli gram negative bacteria was observed as the content of MXene powders in the composite increased.

7- MXene alloy foam displayed Ca and P precipitation when immersed in simulated body fluid; however, no apatite formation was observed even after 25 days mainly due to presence of Fluorene based functional groups formed during etching.

8- Apatite formation was observed in MAX alloy foams after soaking for 15 days in simulated body. The Ca/P ratio was found to be around 1.6, close to that of bone.

Future Studies:

- The effect of starting MAX alloy powder particle size, shape and chemical composition on MXene synthesizing should be investigated to get reproducible MXene powders.
- Surface chemistry of the starting MAX alloys should be clearly identified to determine the surface condition on etching during MXene production.
- Surface termination groups of MXene alloys should be determined so as to reveal the effect of different surface termination groups on antibacterial properties and apatite formation ability.
- Mechanical tests should be employed to MAX and MXene alloy foams to determine their suitability in biomedical application as a graft and implant material.

REFERENCES

[1] TIWARI J. N., TIWARI R. N. and KIM K. S. (2012), “Zero-dimensional, one-dimensional, two-dimensional and three-dimensional nanostructured materials for advanced electrochemical energy devices”, *Progress in Materials Science,* vol. 57, issue 4, pp. 724–803.

[2] SUDHA P. N., SANGEETHA K., VIJAYALAKSHMI K. and BARHOUM A. (2018), “Nanomaterials History, Classification, Unique Properties, Production and Market”, *In Emerging Applications of Nanoparticles and Architectural Nanostructures: Current Prospects and Future Trends,* Ed. Ahmed Barhoum, Abdel Salam Hamdy Makhlouf, pp. 341–384, Elsevier, DOI: 10.1016/B978-0-323-51254-1.00012-9.

[3] VENKATESHALU S. and GRACE A. N. (2020), “MXenes-A new class of 2D layered materials: Synthesis, properties, applications as supercapacitor electrode and beyond”, *Applied Materials Today,* vol. 18, pp. 100509.

[4] QUADRI F. B. (2021), “Zero Dimensional Materials: Properties, Synthesis and Applications A Review”, *Journal of Emerging Technologies and Innovative Research,* vol. 8, issue 8, pp. 92-97.

[5] BAIG N. (2023), “Two-dimensional nanomaterials: A critical review of recent progress, properties, applications, and future directions”, *Composites Part A: Applied Science and Manufacturing,* vol. 165, pp. 107362, DOI: 10.1016/j.compositesa.2022.107362.

[6] AN J., LI G., ZHANG Y., ZHANG T., LIU X., GAO F. and FAN H. (2020), “Recent advances in enzyme-nanostructure biocatalysts with enhanced activity”, *Catalysts,* vol. 10, issue 3, pp. 338, DOI: 10.3390/catal10030338.

[7] ANANDAN V., GANGADHARAN R. and ZHANG G. (2009), “Role of SAM chain length in enhancing the sensitivity of nanopillar modified electrodes for glucose detection”, *Sensors,* vol. 9, issue 3, pp. 1295- 1305.

[8] DUBOIS S. (2020), "Microstructure-oxidation resistance relationship in Ti_3AlC_2 MAX phase", *Journal of Alloys and Compounds*, vol. 826, pp. 154062 DOI: 10.1016/j.jallcom.2020.15406.

[9] BU F., ZAGHO M. M., IBRAHIM Y., MA B., ELZATAHRY A. and ZHAO D. (2020), "Porous MXenes: Synthesis, structures, and application", *Nano Today*, vol. 30, pp. 100803, DOI: 10.1016/j.nantod.2019.100803.

[10] BARSOUM M. W. and RADOVIC M. (2011), "Elastic and Mechanical Properties of the MAX Phases", *Annual Review of Materials Research*, vol. 41, pp. 195–227.

[11] AKHLAGHI M., TAYEBIFARD S. A., SALAHI E., SHAHEDİ ASL M. and SCHMIDT G. (2018), "Self-propagating high-temperature synthesis of Ti_3AlC_2 MAX phase from mechanically activated Ti/Al/graphite powder mixture", *Ceramics International*, vol. 44, issue 8, pp. 9671–9678, DOI: 10.1016/j.ceramint.2018.02.195.

[12] PAZNIAK A., BAZHIN P., SHPLIS N., KOLESNIKOV E., SHCHETININ I., KOMISSAROV A. and POLCAK J. (2019), "$Ti_3C_2T_x$ MXene characterization produced from SHS-ground Ti_3AlC_2", *Materials and Design*, vol. 183, pp. 108143, DOI: 10.1016/j.matdes.2019.108143.

[13] LEI X. and NAIMING L. (2022), "Structure and Synthesis of MAX Phase Materials: A Brief Review", *Critical Reviews in Solid State and Materials Sciences*, vol. 47, issue 5, pp. 736–771, DOI: 10.1080/10408436.2021.1966384.

[14] VENKATESHALU S. and GRACE A. N. (2020), "MXenes-A new class of 2D layered materials: Synthesis, properties, applications as supercapacitor electrode and beyond", *Applied Materials Today*, vol. 18, pp. 100509, DOI: 100509. 10.1016/j.apmt.2019.100509.

[15] SHEKHIREV M., SHUCK C. E., SARYCHEVA A. and GOGOTSI Y. (2021), "Characterization of MXenes at every step, from their precursors to single flakes and assembled films", *Progress in Materials Science*, vol. 120, pp. 100757.

[16] NAGUIB M., KURTOGLU M., PRESSER V., LU J., NIU J., HEON M. and BARSOUM M. W. (2011), "Two-dimensional nanocrystals produced by exfoliation of Ti_3AlC_2", *Advanced Materials*, vol. 23, issue 37, pp. 4248–4253.

[17] TANG H., FENG Y., HUANG X., DOU Y., DING D., XIA M. and ZHANG X. (2017), "Reactive Synthesis of Polycrystalline Ti_3AlC_2 and Its Sintering Behavior", *Rare Metal Materials and Engineering,* vol. 46, issue 8, pp. 2108–2113, DOI: 10.1016/s1875-5372(17)30188-10.

[18] PANDA S., DESHMUKH K., KHADHEER PASHA S. K., THEERTHAGİRİ J., MANİCKAM S. and CHOİ M. Y. (2022), "MXene based emerging materials for supercapacitor applications: Recent advances, challenges, and future perspectives", *Coordination Chemistry,* vol. 462, pp. 214518.

[19] GHIDIU M., LUKATSKAYA M., ZHAO MQ., GOGOTSI Y. and BARSOUM M. W. (2014), "Conductive two-dimensional titanium carbide 'clay' with high volumetric capacitance", *Nature,* vol. 516, pp. 78–81, DOI: 10.1038/nature13970.

[20] GONZALEZ-JULIAN J. (2021), "Processing of MAX phases: From synthesis to applications", *Journal of the American Ceramic Society,* vol. 104, issue 2, pp. 659–690.

[21] NATU V., PAI R., SOKOL M., CAREY M., KALRA V. and BARSOUM M. W. (2020), "2D $Ti_3C_2T_z$ MXene Synthesized by Water-free Etching of Ti_3AlC_2 in Polar Organic Solvents", *Chemistry*, vol. 6, issue 3, pp. 616–630.

[22] Lİ T., YAO L., LIU Q., GU J., LUO R., LI J., YAN X., WANG W., LIU P., CHEN B., ZHANG W., ABBAS W., NAZ R. and ZHANG D. (2018), "Fluorine-free synthesis of high-purity $Ti_3C_2T_x$ (T=OH, O) via alkali treatment", *Angew. Chemie Int. Ed.,* vol. 57, issue 21, pp. 6115–6119, DOI: 10.1016/j.chempr.2020.01.019.

[23] URBANKOWSKI P., ANASORI B., MAKARYAN T., ER D., KOTA S., WALSH P. L., ZHAO M., SHENOV V. B., BARSOUM M. W. and GOGOTSI Y. (2018), "Synthesis of two-dimensional titanium nitride Ti_4N_3 (MXene)", *Nanoscale,* vol. 8, pp. 11385–11391.

[24] VERGER L., XU C., NATU V., CHENG H. M., REN W. and BARSOUM M. W. (2019), "Overview of the synthesis of MXenes and other ultrathin 2D transition metal carbides and nitrides", *Current Opinion in Solid State and Materials Science,* vol. 23, issue 3, pp. 149-163, DOI: 10.1016/j.cossms.2019.02.001.

[25] FENG W., LUO H., WANG Y., ZENG S., TAN Y., ZHANG H. and PENG S. (2018), "Ultrasonic assisted etching and delaminating of Ti_3C_2 MXene", *Ceramics International,* vol. 44, issue 6, pp. 7084–7087.

[26] LUKATSKAYA M. R., KOTA S., LIN Z., ZHAO M. Q., SHPIGEL N., LEVI M. D. and GOGOTSI Y. (2017), "Ultra-high rate pseudocapacitive energy storage in two-dimensional transition metal carbides", *Nature Energy,* vol. 2, issue 8, pp. 1-6.

[27] BOOTA M., ANASORI B., VOIGT C., ZHAO M. Q., BARSOUM M. W. and GOGOTSI Y. (2016), "Pseudocapacitive Electrodes Produced by Oxidant-Free Polymerization of Pyrrole between the Layers of 2D Titanium Carbide (MXene)", *Advanced Materials (Deerfield Beach, Fla.),* vol. 28, issue 7, pp. 1517–1522.

[28] VERGER L., NATU V., CAREY M. and BARSOUM M. W. (2019), "MXenes: An Introduction of Their Synthesis, Select Properties, and Applications." *Trends in Chemistry,* vol. 1, issue 7, pp. 656-669.

[29] JIANG X., KUKLIN A. V., BAEV A., GE Y., ÅGREN H., ZHANG H. and PRASAD P. N. (2020), "Two-dimensional MXenes: From morphological to optical, electric, and magnetic properties and applications", *Physics Reports,* vol. 848, pp. 1-58, DOI: 10.1016/j.physrep.2019.12.006.

[30] FU B., SUN J., WANG C., SHANG C., XU L., LI J. and ZHANG H. (2021), "MXenes: Synthesis, Optical Properties, and Applications in Ultrafast Photonics", *Small,* vol.17, issue 11, pp. 2006054, DOI: .1002/smll.202006054.

[31] MALEKI A., GHOMI M., NIKFARJAM N., AKBARI M., SHARIFI E., SHAHBAZI M. A. and CHEN Y. (2022), "Biomedical Applications of MXene-Integrated Composites: Regenerative Medicine, Infection Therapy, Cancer Treatment, and Biosensing", *Advanced Functional Materials,* vol. 32, issue 34, pp. 2203430, DOI: 10.1002/adfm.202203430.

[32] FU Y., ZHANG J. B., LIN H. and MO A. (2021), "2D titanium carbide (MXene) nanosheets and 1D hydroxyapatite nanowires into free standing nanocomposite membrane: in vitro and in vivo evaluations for bone regeneration", *Materials Science and Engineering C,* vol. 118, pp. 111367, DOI: 10.1016/j.msec.2020.111367.

[33] XU B., ZHU M., ZHANG W., ZHEN X., PEI Z., XUE Q., ZHI C. and SHI P. (2016), “Ultrathin MXene-Micropattern-Based Field-Effect Transistor for Probing Neural Activity”, *Advanced Material,* vol. 28, issue 17, pp. 3333-3339.

[34] LIU Z., ZHAO M., LIN H., DAI C., REN C., ZHANG S., PENG W. and CHEN Y. (2018), “2D Magnetic Titanium Carbide MXene for Cancer Theranostics”, *Journal of Materials Chemistry B,* vol. 6, issue 21, pp. 3541–3548.

[35] LIN H., CHEN Y. and SHI J. (2018), “Insights into 2D MXenes for Versatile Biomedical Applications: Current Advances and Challenges Ahead”, *Advanced Science,* vol. 5, issue 10, pp. 1800518, DOI: 10.1002/advs.201800518.

[36] SHUCK C. E., HAN M., MALESKI K., HANTANASİRİSAKUL K., KİM, S. J., CHOİ J. and GOGOTSİ Y. (2019), “Effect of Ti_3AlC_2 MAX Phase on Structure and Properties of Resultant $Ti_3C_2T_x$ MXene”, *ACS Applied Nano Materials,* vol. 2, issue 6, pp. 3368–3376.

[37] LIM K. R. G., SHEKHIREV M., WYATT B. C., ANASORI B., GOGOTSI Y. and SEH Z. W. (2022), “Fundamentals of MXene Synthesis”, *Nature Synthesis,* vol. 1, issue 8, pp. 601–614.

[38] IBRAGIMOVA R., ERHART P., RINKE P. and KOMSA H. P. (2021), “Surface Functionalization of 2D MXenes: Trends in Distribution, Composition, and Electronic Properties”, *Journal of Physical Chemistry Letters,* vol. 12, issue 9, pp. 2377–2384.

[39] RASOOL K., HELAL M., REN C. E. and GOGOTSI Y. (2016), “Antibacterial Activity of $Ti_3C_2T_x$ MXene”, *ACS Nano,* vol. 10, issue 3, pp. 3674-3684.

[40] RONALD N. J., CHARLES H. B. and DOUGLAS J. B. (2001), “Multi-laboratory assessment of the linezolid spectrum of activity using the Kirby-Bauer disk diffusion method: Report of the Zyvox® Antimicrobial Potency Study (ZAPS) in the United States”, *Diagnostic Microbiology and Infectious Disease,* vol. 40, issue 1-2, pp. 59-66.